Melt inclusion record of the conditions of ascent, degassing, and extrusion of volatile-rich alkali basalt during the powerful 2002 flank eruption of Mount Etna (Italy)

N. Spilliaert,[1] P. Allard,[1,2] N. Métrich,[1] and A. V. Sobolev[3]

Received 7 July 2005; revised 29 September 2005; accepted 18 January 2006; published 25 April 2006.

[1] Two unusual, highly explosive flank eruptions succeeded on Mount Etna in July August 2001 and in October 2002 to January 2003, raising the possibility of changing magmatic conditions. Here we decipher the origin and mechanisms of the second eruption from the composition and volatile (H_2O, CO_2, S, Cl) content of olivine-hosted melt inclusions in explosive products from its south flank vents. Our results demonstrate that powerful lava fountains and ash columns at the eruption onset were sustained by closed system ascent of a batch of primitive, volatile-rich ($\geq$4 wt %) basaltic magma that rose from $\geq$10 km depth below sea level (bsl) and suddenly extruded through 2001 fractures maintained opened by eastward flank spreading. This magma, the most primitive for 240 years, probably represents the alkali-rich parental end-member responsible for Etna lavas' evolution since the early 1970s. Few of it was directly extruded at the eruption onset, but its input likely pressurized the shallow plumbing system several weeks before the eruption. This latter was subsequently fed by the extrusion and degassing of larger amounts of the same, but slightly more evolved, magma that were ponding at 6–4 km bsl, in agreement with seismic data and with the lack of preeruptive SO_2 accumulation above the initial depth of sulphur exsolution ($\sim$3 km bsl). We find that while ponding, this magma was flushed and dehydrated by a CO_2-rich gas phase of deeper derivation, a process that may commonly affect the plumbing system of Etna and other alkali basaltic volcanoes.

Citation: Spilliaert, N., P. Allard, N. Métrich, and A. V. Sobolev (2006), Melt inclusion record of the conditions of ascent, degassing, and extrusion of volatile-rich alkali basalt during the powerful 2002 flank eruption of Mount Etna (Italy), *J. Geophys. Res.*, *111*, B04203, doi:10.1029/2005JB003934.

1. Introduction

[2] Volatile components play a key role in the dynamics of ascent and eruption of magmas, in spite of their relatively minor mass fraction. This results from their ability to gradually exsolve from the melt and to form a separate gas phase whose expansion, upon decompression, converts part of the thermal magmatic energy into mechanical energy. Moreover, the differing pressure-dependent solubilities of the volatile species (H_2O, CO_2, S, Cl, F, etc.) result in progressive compositional changes of the gas phase in function of the depth and the dynamics of magma degassing. Hence, knowing the pressure-related evolution of dissolved and exsolved volatiles in a magma can provide key information on its path(s) of ascent, degassing and eruption. It is also essential to interpret the compositional changes in gas emissions at the surface which, in complement to other parameters, can help understand and possibly forecast the evolution of a volcanic eruption.

[3] Such information can be retrieved by probing melt droplets that are trapped during crystal growth and preserved as glass inclusions upon cooling [e.g., *Anderson*, 1974; *Roedder*, 1984; *Sobolev*, 1996]. These tiny inclusions (a few tens to a few hundred microns) entrapped in crystals can yield a detailed record of the preeruptive evolution of the bulk magma, provided that they are representative enough and well preserved. In basaltic systems, the most favorable conditions are offered by melt inclusions that are trapped in early formed olivine crystals and that are recovered in rapidly quenched products from explosive volcanic activity.

[4] Mount Etna, in Sicily, is one remarkable laboratory volcano where magma degassing processes and the role of volatiles in eruptive mechanisms can be investigated from the study of olivine-hosted melt inclusions. First, Mount Etna is a very active and intensively surveyed volcano that produces both effusive and explosive eruptions of alkali basalts-trachybasalts. These lavas derive from the partial melting of upwelling asthenosphere [*Tonarini et al.*, 2001; *Schiano et al.*, 2001] and rise through deep faults cutting a $\sim$20 km thick continental crust [e.g., *Laigle et al.*, 2000].

[1] Laboratoire Pierre Süe, CNRS-CEA, Saclay, France.
[2] Istituto Nazionale di Geofisica e Vulcanologia, Catania, Italy.
[3] Max-Planck-Institut für Chemie, Mainz, Germany.

0148-0227/06/2005JB003934$09.00

Their conditions of ascent, degassing and eruption can be reliably tracked by combining crystal melt inclusion studies with data obtained by the multidisciplinary monitoring network developed by INGV (Catania, Italy). Second, Mount Etna is one of the strongest emitters of magma-derived volatiles on Earth, releasing huge amounts of gas during its eruptions but also during continuous open-conduit magma degassing across its summit craters [*Allard et al.*, 1991; *Allard*, 1997; *Caltabiano et al.*, 1994, 2004]. As a matter of fact, previous melt inclusion studies have revealed that Etna alkali basaltic magmas are abnormally rich in water, sulphur and halogens compared to alkali basalts elsewhere [*Métrich and Clocchiatti*, 1989; *Clocchiatti et al.*, 1992; *Métrich et al.*, 1993, 2004]. This feature can be related to the very peculiar setting of the volcano, at the collision boundary of African and European continental plates and in the foreground of slab subduction under the Aeolian volcanic arc [*Barberi et al.*, 1974; *Gvirtzamn and Nur*, 1999].

[5] Since the early 1970s, the lava production rate of Etna has increased by a factor of 4 and the erupted lavas have shown an unprecedented gradual increase of their alkali content [e.g., *Clocchiatti et al.*, 1988; *Tanguy et al.*, 1997] and selected (Sr, B) isotopic ratios [e.g., *Condomines et al.*, 1995; *Tonarini et al.*, 2001], while becoming more and more basic. It has recently been verified [*Métrich et al.*, 2004; *Clocchiatti et al.*, 2004] that these compositional changes were due to the input of a new, alkali-richer basaltic-trachybasaltic magma that has gradually mixed with and replaced the alkali-poorer magmas previously filling the volcano plumbing system. In particular, this recent change in Etna magma feeding system was elucidated from a detailed study of olivine melt inclusions in unusually primitive basalt that was extruded during a violent flank eruption in July–August 2001 [*Métrich et al.*, 2004].

[6] Only fourteen months after this 2001 event, Mount Etna suddenly erupted again and delivered a still more explosive and longer flank eruption that lasted from 26 October 2002 to 28 January 2003. Like the 2001 event, this second eruption was unusual in its high explosivity and in the simultaneous extrusion of two distinct magma types on the southern and northern flanks of the volcano, including primitive trachybasalts that contained uncommon amphibole phenocrysts and quartz arenite crustal xenoliths [*Clocchiatti et al.*, 2004; *Andronico et al.*, 2005]. Moreover, it was accompanied by strong seismicity [*Gambino et al.*, 2004] and extensive (meter-sized) ground movements along volcano-tectonic faults on the northern and eastern slopes of Etna, due to eastward flank spreading [*Acocella et al.*, 2003; *Neri et al.*, 2005]. These different aspects have raised an intense debate as regards the possible triggering mechanism of this second flank eruption and its significance for the magma plumbing system. Whether it was triggered by magma overpressuring from depth [*Gambino et al.*, 2004; *Aloisi et al.*, 2003; *Patanè et al.*, 2003] or, rather, by decompression due volcano-tectonic spreading [*Neri et al.*, 2005; *Monaco et al.*, 2005] has contrasted implications for the preeruptive conditions of the plumbing system and for the dynamics of magma ascent and eruption.

[7] In order to address this question and to elucidate the conditions of magma ascent, storage and degassing before and during the 2002–2003 flank eruption of Etna, we have carried out detailed investigations of the chemistry and the volatile content of its bulk products and their olivine-hosted melt inclusions. We collected both explosive and effusive products of the eruption on several occasions, since its beginning and during its most energetic phases until mid-December 2002. We report and discuss here the most comprehensive data set yet obtained for melt inclusions on Etna, with the first systematic determination of H_2O, CO_2, S, Cl and boron dissolved in same series of inclusions. The results allow us to infer the depth of ascent of the new magma and to model its conditions of degassing and eruption. They also provide further information on the recent evolution of Mount Etna feeding system and can serve to interpret the composition of gas emissions measured during the eruption [*Burton et al.*, 2003b; *Andronico et al.*, 2005]. Finally, they bear broader implications for alkali basaltic volcanism.

2. Volcanological Framework

[8] The 2001 and 2002–2003 flank eruptions of Etna were preceded by several years of increasing and quite exceptional summit eruptive activity. After a massive flank eruption in 1991–1993, the largest eruption in the last three centuries, and a period of rest until mid-1995, continuous magma refilling was manifested in progressive dilatation of the volcanic pile and associated seismicity [*Bonaccorso and Davis*, 2004]. Gradual ascent of fresh magma in the central conduit system resulted in successive stages of violent eruptive activity at the four summit craters in the period 1995–2001 [*Corsaro and Pompilio*, 2004a]. These included powerful lava fountains in 1995 (Northeast crater) and 1998–2001 (Southeast crater, SEC) [*Alparone et al.*, 2004], a sub-Plinian paroxysmal event on 22 July 1998 (Voragine crater), and the first terminal eruption at Bocca Nuova crater in November–December 1999 [*Calvari et al.*, 2003].

[9] The July–August 2001 flank eruption started in coincidence with the ultimate fountains at SEC, after four days of intense seismicity and fracturing of the south flank of Etna that were generated by vertical dike intrusion from 3 to 5 km depth below sea level (bsl) [*Patanè et al.*, 2003; *Acocella and Neri*, 2003; *Behncke and Neri*, 2003]. This brief (23 days) but highly explosive eruption emitted, through its lower vents, an uncommon plagioclase-poor basalt-trachybasalt, containing abundant sedimentary xenoliths and amphibole megacrysts [*Pompilio and Rutherford*, 2002; *Clocchiatti et al.*, 2004]. A detailed study of melt inclusions trapped in its olivine crystals has revealed its direct derivation from a new alkali- and volatile-rich basaltic magma that has invaded Mount Etna plumbing system since the early 1970s [*Métrich et al.*, 2004].

[10] After several months of quiescence, seismic swarms and ground deformations registered since February 2002 evidenced a new refilling of the shallow magma plumbing system [*Gambino et al.*, 2004]. Volcanic activity at the summit craters renewed in March 2002 and lasted until 22 September, when a strong earthquake swarm occurred on the Pernicana transcurrent fault that borders the eastern flank of Etna to the north [*Neri et al.*, 2004]. Then, in the night of 26–27 October 2002, an eruption started suddenly on both the upper south and north flanks of the volcano

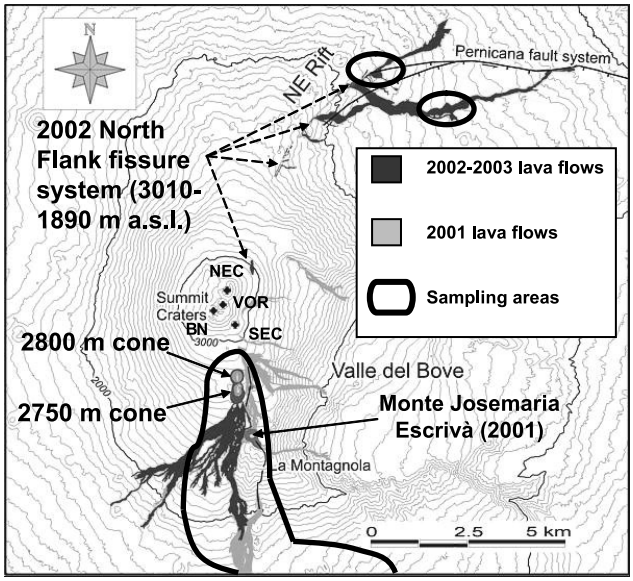

Figure 1. Location of 2750 m and 2800 m eruptive cones and map of lava flows from both July-August 2001 and 2002–2003 eruption of Mount Etna. Modified from *Neri et al.* [2004] with permission.

(INGV Web site reports, Catania, Italy, Oct. 2002) after only a few hours of intense precursory seismicity [*Patanè et al.*, 2003]. A 1-km-long N-S eruptive fracture first opened between 2850 and 2600 m above sea level (asl) on the south flank, producing 100–300 m high fire fountaining that rapidly evolved into a 2 km high ash column. Soon after, another eruptive fracture opened on the northeast flank (3010–2920 m asl) which, after a very brief phase of fountaining, propagated downslope (between 2500 and 1890 m asl) along the NE Rift during the next 2 days (Figure 1). This fracture propagation was accompanied by several tens of centimeters of E-W thrust movement along the Pernicana fault and gave rise to violent spattering, cone building and the extrusion of about 10×10^6 m^3 of lava flows that buried the northern tourist settlements on Etna [*Behncke and Neri*, 2003]. However, this north flank eruptive activity rapidly ended on 5 November, whereas on the south flank the eruption continued for 94 days, until 28 January 2003 [*Andronico et al.*, 2005]. Three distinct phases can be distinguished in its sequence on basis of field observations and variations of seismic tremor and SO_2 emission rate (Figures 2a–2c).

2.1. Phase I (26 October to 12 November)

[11] This initial phase of the eruption was very powerful and marked by the sharpest increase in seismic tremor amplitude (Figure 2b). The first two days were characterized by an alternation of fire fountaining and phreatomagmatic explosions from three vents. These rapidly gave rise to 5–6 km high dense ash columns which generated heavy ash falls over Catania city and surrounding areas, strongly disturbing public life and air traffic. Between 28 and 31 October, fire fountaining became continuous and very intense (up to 600 m height), while a small amount ($\sim 10^6$ m^3) of lava flows was outpoured. In the same time, voluminous amounts of sulphur dioxide (up to 2×10^7 kg d^{-1}) were released (Figure 2c) [*Andronico et al.*, 2005]. Then, between 1 and 11 November, the eruptive activity concentrated at a new cone forming at 2750 m elevation. There was no more lava effusion, but a sustained explosive activity producing voluminous ash emissions due to intense magma fragmentation. This activity and the SO_2 output showed a smooth decrease until 12 November when, by 1200 UT, the ash plume emissions suddenly disappeared and were replaced by transparent gas emissions accompanying 24 hours of purely Strombolian activity.

2.2. Phase II (12 November to 9 December)

[12] On 13 November, both explosive ash emissions and lava flows resumed at the 2750 m cone (Figure 2a), while increasing SO_2 emission indicated a new magma upsurge in the feeding dike. After a week of fluctuations from fire fountaining to Strombolian explosions, the intensity of explosive manifestations and the rate of lava flow extrusion displayed an increasing trend, associated with enhanced seismic tremor (Figure 2b), that peaked between 24 and 30 November. At that time, the bulk SO_2 flux reached the highest value ever measured on Etna (3×10^7 kg d^{-1};

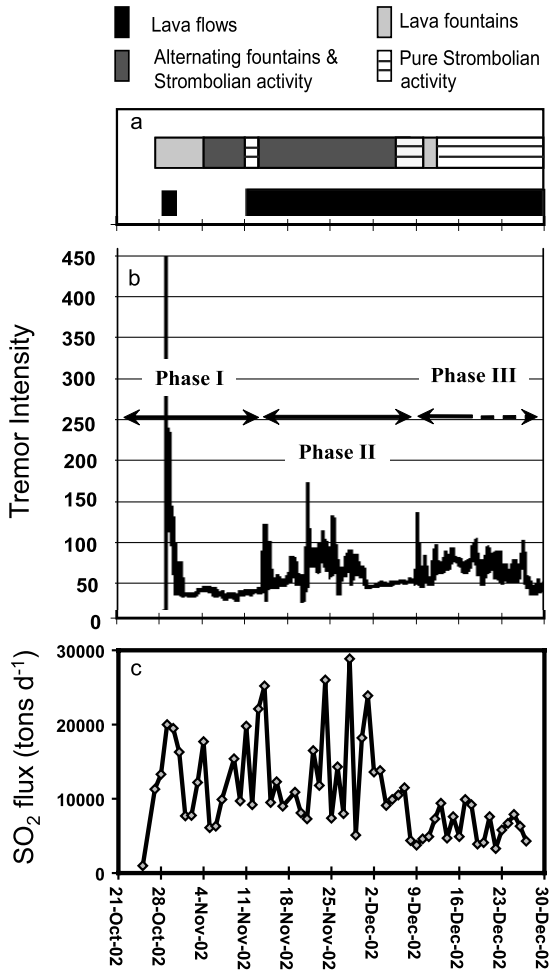

Figure 2. Eruptive phases recognized on basis of (a) field observations of explosive activity (upper bar) and lava flows (lower bar), (b) variations of the seismic tremor, and (c) SO_2 emission rate [*Andronico et al.*, 2005; INGV Web site].

Table 1. Selected Etna 2002 Whole Rock Compositions[a]

	South Flank								North Flank	
	28 Oct	28 Oct	29 Oct	15 Nov	21 Nov	23 Nov	9 Dec	16 Dec	30 Oct	4 Nov
Sample	lava	lapilli[b]	scoriae[b]	scoriae	lapilli[b]	lava	lapilli[b]	lava	lava	lava
SiO_2	46.88	47.11	46.74	47.53	47.15	47.68	47.54	47.62	47.87	48.16
TiO_2	1.77	1.74	1.69	1.66	1.62	1.68	1.66	1.67	17.71	18.23
Al_2O_3	17.25	16.88	15.94	17.17	15.65	17.16	16.88	17.16	1.62	1.62
Fe_2O_3	11.62	11.83	11.87	11.31	11.62	11.29	11.22	11.23	11.11	10.70
MnO	0.17	0.18	0.17	0.17	0.18	0.17	0.18	0.17	0.18	0.17
MgO	5.4	6.26	7.14	5.69	7.53	5.59	5.89	5.51	5.02	4.65
CaO	11.38	11.32	11.75	10.71	11.73	10.91	10.92	10.89	10.16	9.92
Na_2O	3.28	3.25	3.01	3.46	2.97	3.46	3.42	3.46	3.85	4.03
K_2O	1.96	1.91	1.76	2.00	1.75	1.99	2.01	2.06	2.13	2.19
P_2O_5	0.46	0.48	0.43	0.5	0.44	0.48	0.49	0.5	0.56	0.55
LOI	−0.4	−0.61	−0.52	−0.21	−0.37	−0.42	−0.22	−0.28	−0.24	−0.22
Total	99.77	100.35	99.98	99.99	100.21	99.99	99.99	99.99	99.97	100.00
S	<0.01	<0.01	0.017	0.01	0.017	<0.01	0.014	0.011	<0.01	0.014
Cl	0.10	0.09	0.09	0.13	0.10	0.12	0.11	0.11	0.11	0.11
Th	nd	nd	5.7	7.1	6.0	7.0	7.0	7.2	8.6	nd
Rb	nd	nd	43.0	48.0	43.4	47.7	48.7	49.5	49.1	nd
Nb	nd	nd	35.0	40.3	34.8	39.7	40.5	41.3	49.8	nd
La	nd	nd	47.0	53.7	47.3	52.3	53.1	54.2	59.0	nd
Cr	nd	nd	78.6	41.1	75.9	47.3	55.1	52.8	27.6	nd
Ni	nd	nd	52.8	35.2	51.6	36.1	36.2	37.0	25.4	nd
Co	nd	nd	46.7	38.2	44.8	38.4	40.1	38.9	35.5	nd
CaO/Al_2O_3	0.66	0.67	0.74	0.62	0.75	0.64	0.65	0.63	0.57	0.54
S/Cl	nd	nd	0.19	0.07	0.17	nd	0.12	0.10	nd	0.13
Rb/Th	nd	nd	7.5	6.8	7.2	6.8	6.9	6.8	5.7	nd

[a]Major oxides (wt %) were analyzed by ICP-AES, Th, Rb, Nb, La, Cr, Ni, and Co (wt ppm) by ICPMS, and S and Cl (wt %) by specific techniques (CRPG, France).
[b]Samples studied for olivine-hosted melt inclusions; LOI, loss of ignition; nd, not determined.

Figure 2c) and the explosive activity extended upward to a new cinder cone that rapidly built up at 2800 m asl. This new cone became the principal source of ash-rich explosive activity and abundant lava flows (4 km maximum length) until 8–9 December, when a return to purely Strombolian activity was accompanied by a marked drop in the SO_2 output.

2.3. Phase III (10 December 2002 to 28 January 2003)

[13] On 10 December, the eruptive activity migrated back to the 2750 m cone where fire fountaining and lava outpouring, associated with enhanced seismic tremor, temporarily renewed. However, from 10 December onward, the eruption showed a gradual though irregular decline in intensity, with both flattening effusive and explosive activities that generated lower and discontinuous ash columns. It finally ended on 28 January 2003, after one month of slowing mild Strombolian activity and lava effusion from the 2750 m cone.

[14] The total amount of lava and tephra erupted from the south flank vents was estimated to be $20–30 \times 10^6$ m^3 and $40–50 \times 10^6$ m^3, respectively [*Andronico et al.*, 2005]. If one adds the volume of pyroclasts forming the (~150 m high) 2750 and 2800 m cones, then the total amount of erupted tephra might approach 60×10^6 m^3. As a whole, this results in an unusually high explosivity index of ~0.6 for that eruption.

3. Sampling and Analytical Procedures

3.1. Sample Description

[15] In addition to lava flow samples from the north vents, we repeatedly collected the products erupted by effusive and explosive activities at the south vents until 16 December 2002 (Figure 1). Our sample set includes bulk rocks from lava flows, scoriae blocks, and deposits of scoriae and centimeter-sized lapilli produced by lava fountains and Strombolian activity at the 2750 and 2800 m cones. These latter materials were especially suitable for melt inclusion studies owing to their rapid cooling upon eruption. In particular, we focused attention on a series of scoriae and lapilli produced during the most energetic first and second phases of the eruption: 27–29 October and 11 November (phase I), 21 November and 9 December (phase II).

3.2. Analytical Procedures

[16] Lava and scoriae were powdered and their bulk compositions (Table 1) were determined by ICP-AES for major elements, ICP-MS for trace elements and other specific techniques for S, Cl and F at CRPG (SARM, Nancy, France). After gentle grinding of scoriae and lapilli from the six selected deposits, 140 crystals, from the 1–2 mm and 0.5–1 mm grain size fractions, were embedded in epoxy, polished and studied.

[17] Electron microprobe analyses of olivine crystals were performed using a SX50 CAMECA (Service Camparis, Jussieu, France) with 10 to 40 nA beam current and 10 to 100 s counting time. Major elements in melt inclusions, glass embayments and matrix glasses were then analyzed with 10 nA beam current, 10 μm spot size, and counting time of 10 to 25 s. Sulphur, chlorine and phosphorus analyses were carried out with 30 nA beam current, 15 μm spot size, counting times of 100 to 200 s and were checked against internal reference glasses (ALV981R23: S = 1100 ± 70 ppm; Vg2: S = 1460 ± 75 ppm, Cl = 305 ±

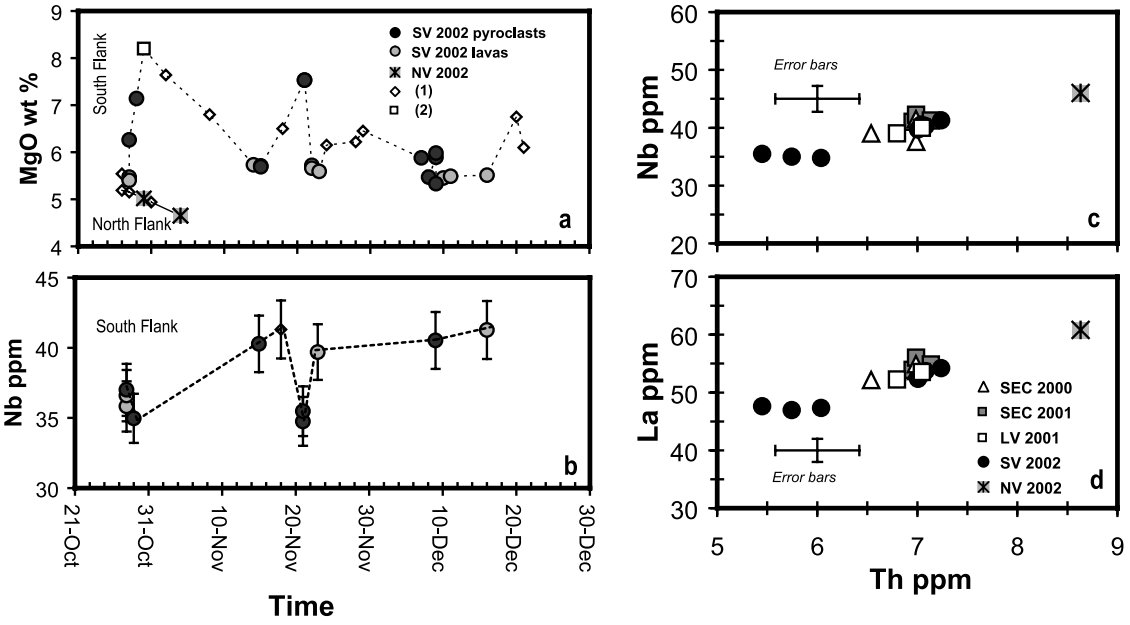

Figure 3. Temporal variations of (a) MgO and (b) Nb in the 2002 bulk lavas and pyroclasts erupted at the South (SV) and North (NV) vents. Evolution of (c) Nb and (d) La against Th in whole rocks. Data for the 2001 flank eruption at lower vents (LV [*Métrich et al.*, 2004]) and lava fountains of May–June 2000 and June–July 2001 at SEC [*Spilliaert*, 2006] are reported for comparison. Other data sources are (1) *Clocchiatti et al.* [2004] and (2) R. A. Corsaro (personal communication, 2005).

30 ppm, P = 954 ± 45 ppm; KE12: Cl = 3280 ± 120 ppm). These values are in agreement with previously published values [*Métrich et al.*, 2001]. We took into account the shift of sulphur Kα X-ray due to the high proportion of sulphates in water-rich, primitive melt inclusions, whereas sulphur was analyzed as S^{II-} in water-poor glasses.

[18] Carbon concentrations were determined with the LPS nuclear microprobe, using the $^{12}C(d, p)^{13}C$ nuclear reaction. The samples were irradiated with deuterons at 1.45 MeV incident energy, and protons were detected after an Al filter of 9 μm, using an annular diode (1500μm depleted zone). The carbon region (between 2.3 and 2.7 MeV) was selected in order to avoid surface contamination. The contribution of the (d, p) reactions on Si, Mg, Al of the matrix to that carbon region was assessed by systematically analyzing a carbon-free Etna glass, with a total integrated charge of 10 to 15 μC, and was subtracted from the sample spectra. The matrix effect was calculated using PYROLE [*Trouslard*, 1995]. Analyses of glasses and melt inclusions were made in the scanning mode (10 × 10 to 30 × 30 μm^2 depending of the sample dimensions) in order to avoid beam damage. The integrated charge varied from 1 to 3 μC, implying a minimum detection limit between 40 and 15 ppm C (i.e., ∼150 to 55 ppm CO_2). Carbon concentrations were calibrated against a scapolite standard (6800 ppm C) and a water-bearing Etna basaltic glass containing 300 ± 30 ppm C [*Métrich et al.*, 2004]. Systematic analysis of this internal reference glass indicated 310 ± 30 ppm C.

[19] The water and boron contents of the same inclusions were determined with a CAMECA IMS3f ion microprobe in Max-Planck-Institut für Chemie (Mainz, Germany). All measurements were made using an O^- primary beam, 10 nA beam current, 15–20 μm beam size and ^{30}Si as internal standard [*Sobolev and Chaussidon*, 1996]. Titanium was used as internal reference element to verify the reliability of each analysis and the lack of host olivine contribution (that would have resulted in Ti dilution). Calibration for boron was made using basaltic to rhyolitic standards containing from 0.34 to 940 ppm B. While a good consistency for B content ≤10 ppm was found with previous inclusion data for Etna basalt [*Schiano et al.*, 2001], higher contents tend to be overestimated owing to matrix effects in B-rich rhyolitic standards and, so, were not

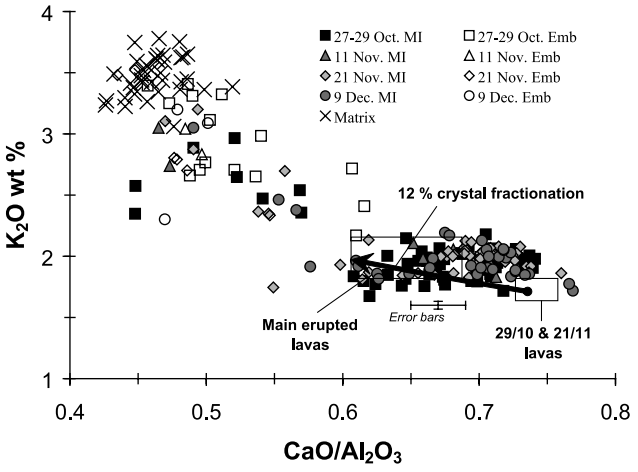

Figure 4. K_2O versus CaO/Al_2O_3 ratio in olivine-hosted melt inclusions (MI), glass embayments (Emb), matrix glasses and bulk rocks (white domains) from the south vents of the 2002 eruption. The predominant erupted magma ($CaO/Al_2O_3 < 0.70$) is derived by 12% crystal fractionation from the most primitive magma extruded on 29 October and 21 November (see text).

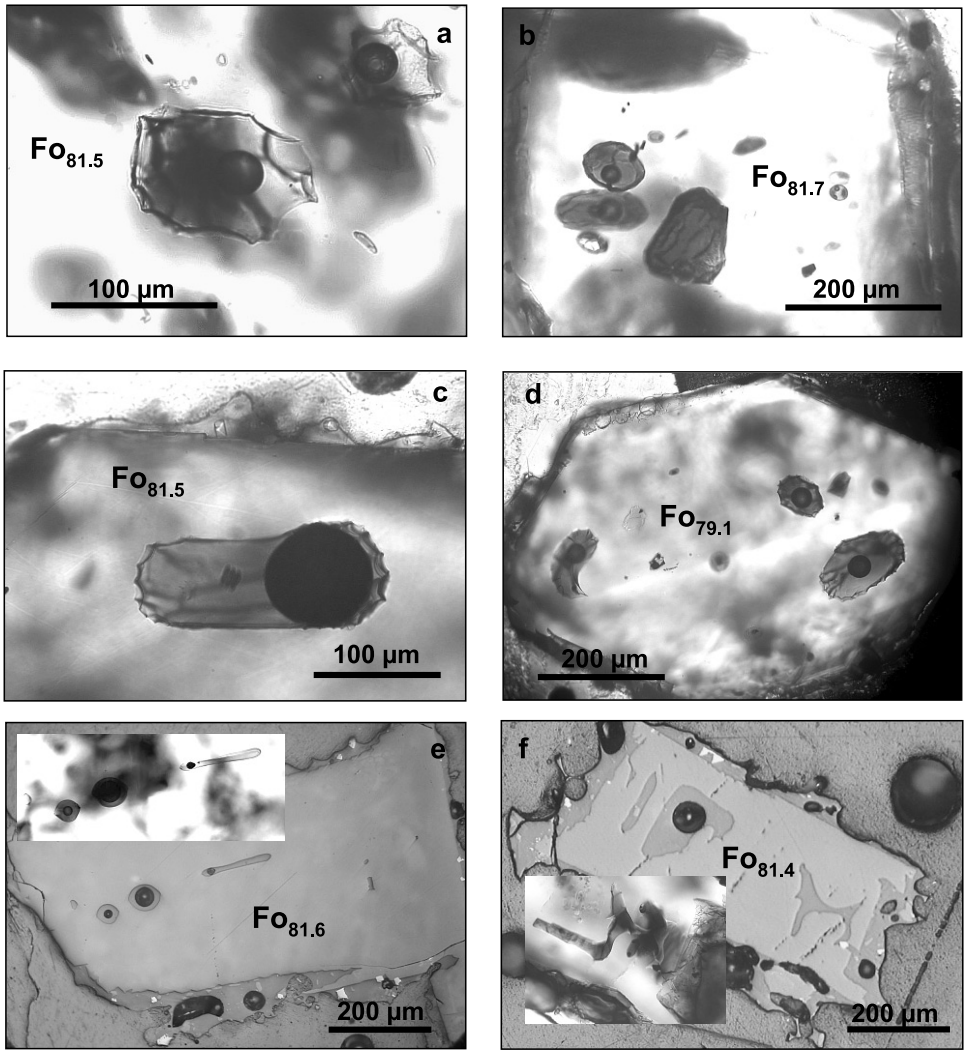

Figure 5. Photomicrographs of olivines, their melt inclusions, and glass embayments for (a) and (b) typical primitive melt inclusions in olivines from 29 October and 21 November 2002 samples, with a bubble volume fraction (V_B/V_{MI}) between ~0.04 and 0.08, (c) melt inclusion with a larger bubble ((V_B/V_{MI}) > 0.10–0.20), (d) inclusions with variable bubble volume fractions, (e) necking down feature indicative of heterogeneous gas/melt trapping in 21 November sample, and (f) embayments (glass reentrants) formed during crystal growth, either isolated or still connected with the groundmass. Figures 5a, 5b, 5c, 5d, 5e, and 5f correspond to olivines ET02-5-41, 24-17, 5-25, 5-5, 24-7, and 24-22, respectively, whose melt inclusion compositions are reported in Table 2. Fo is the fosterite content of host olivine (Fo = [100 × Mg/(Fe + Mg)] in mol %).

considered. For H_2O, we used synthetic glass standards equivalent in composition to Etna lava and containing 1.19, 1.47, 3.04 and 3.60 wt % H_2O (B. Scaillet, ISTO, France). These synthetic glasses were previously used for water calibration during electron microprobe analysis and to calculate the H_2O molar absorptivity coefficient during Fourier Transform infrared analysis of melt inclusions. Consequently, our present SIMS results can be directly compared with H_2O data recently obtained with these methods on previous Etna samples [*Métrich et al.*, 2004].

4. Results

4.1. Whole Rock Chemistry

[20] Bulk lavas from the north and south vents markedly differ in their mineralogy but also in their chemical composition (Table 1). The NE Rift lavas are common, plagioclase-rich Etnean trachybasalts containing ~30 vol % of phenocrysts [*Clocchiatti et al.*, 2004; *Andronico et al.*, 2005]. They are relatively poor in MgO (<5 wt %, Figure 3a) and transition elements (Table 1), and have rather high contents of alkalis, La, Nb and Th (Figures 3c–3d). In contrast, lavas and scoriae from the south vents contain no plagioclase phenocrysts and only ~15–20% of pyroxene and olivine phenocrysts, plus rarer amphiboles [*Clocchiatti et al.*, 2004; *Andronico et al.*, 2005]. Most of them have a quite uniform chemical composition, at the limit between basalts and trachybasalts (referred as trachybasalts hereafter), with on average 5.7 wt % MgO, 7.2 ppm Th, 40 ppm Nb and 53 ppm La (Figures 3a–3d). They are closely similar to the products

Table 2. Selected Compositions of Melt Inclusions, Glass Embayments and Matrix Glasses From the 2002 Eruption

Sample[a]	Fo,[b] mol %	PEC[c]	SiO_2, wt %	TiO_2, wt %	Al_2O_3, wt %	FeO,[d] wt %	MnO, wt %	MgO, wt %	CaO, wt %	Na_2O, wt %	K_2O, wt %	P_2O_5, wt %	CaO /Al_2O_3	B, ppm	S, wt %	Cl, wt %	S/Cl	H_2O, wt %	CO_2,[e] ppm	P,[f] MPa
27–28 October (ET02-7 and 8)																				
8-2a	80.8	0%	44.80	2.00	16.71	9.17	0.24	5.52	11.78	3.15	2.18	0.61	0.70	9.4	0.347	0.158	2.19	2.7	2330	330
7-5c	81.7	3%	45.31	1.78	15.92	9.70	0.18	6.24	11.38	3.20	1.96	0.55	0.71	8.6	0.312	0.163	1.91	2.7	2360	330
8-5a	81.4	2%	44.98	1.91	15.92	10.01	0.14	6.31	10.58	3.20	1.89	0.57	0.66	7.8	0.327	0.143	2.29	3.5	1530	300
8-28b	82.4	0%	44.46	2.26	16.54	8.95	0.12	5.81	11.06	3.07	1.89	0.43	0.67	7.7	0.292	0.159	1.83	3.6	1135	265
7-6	82.1	2%	44.85	1.80	15.91	9.41	0.20	6.18	11.15	3.46	1.99	0.59	0.70	8.6	0.313	0.160	1.96	2.9	1250	235
8-3b	81.3	2%	44.77	1.82	15.87	9.55	0.20	5.98	11.54	3.34	2.06	0.61	0.73	8.8	0.322	0.144	2.23	2.8	1240	230
8-28a	82.4	1%	43.71	2.36	16.57	9.87	0.19	6.25	11.19	3.12	1.77	0.43	0.68	7.4	0.285	0.159	1.79	3.5	770	220
8-15a	82.0	0%	43.95	1.71	16.15	9.81	0.18	6.02	10.89	3.22	1.98	0.47	0.67	8.4	0.294	0.153	1.92	3.3	780	205
8-4	80.7	2%	44.80	1.74	15.96	10.42	0.20	6.25	11.19	3.22	1.89	0.58	0.70	8.4	0.287	0.144	1.99	3.1	630	175
8-11	78.9	1%	48.41	1.61	18.36	8.75	0.18	4.43	8.22	4.30	2.35	0.75	0.45	nd	0.147	0.202	0.73	1.3	385	75
7-1a	81.1	Emb	48.39	1.74	17.86	9.57	0.20	3.74	9.66	4.62	2.65	0.68	0.54	nd	0.144	0.207	0.69	0.8	270	40
29 October (ET02-5)																				
5-41b	81.5	2%	45.00	1.86	15.82	9.34	0.18	5.92	11.27	2.87	1.91	0.57	0.71	8.9	0.309	0.163	1.90	3.3	2795	400
5-42	80.0	0%	44.81	1.99	16.82	9.53	0.14	5.60	11.13	3.16	1.99	0.53	0.66	7.7	0.292	0.141	2.07	3.2	2280	350
5-17a	79.2	0%	44.83	1.81	15.86	9.69	0.19	5.48	11.75	3.01	1.98	0.55	0.74	8.5	0.307	0.152	2.02	3.5	1745	320
5-5	79.1	0%	44.57	1.78	16.08	9.41	0.15	5.39	11.41	3.00	1.93	0.57	0.71	8.4	0.301	0.151	1.99	3.6	1635	315
5-41a	81.5	3%	44.80	1.84	16.16	9.39	0.15	5.96	11.18	3.07	1.94	0.57	0.69	8.7	0.295	0.160	1.85	3.2	1860	310
5-40	82.4	2%	44.41	1.73	15.47	9.42	0.17	6.32	10.81	3.14	1.79	0.58	0.70	7.6	0.300	0.153	1.96	3.4	1610	300
5-1a	79.0	0%	44.80	1.73	15.93	9.60	0.15	5.20	11.68	3.15	1.92	0.57	0.73	8.3	0.299	0.153	1.95	3.4	1580	295
5-25b	81.5	1%	44.27	1.94	17.09	9.20	0.21	5.77	10.81	3.57	2.00	0.59	0.63	8.4	0.285	0.146	1.96	3.3	1435	275
5-15b	80.9	0%	44.45	1.85	15.94	9.47	0.14	5.71	11.34	2.96	1.92	0.53	0.71	8.1	0.285	0.145	1.97	3.6	1230	275
5-39	82.5	3%	44.07	1.88	15.75	9.42	0.24	6.38	11.03	3.16	1.91	0.58	0.70	8.2	0.319	0.163	1.96	3.2	1145	240
5-30b	81.8	2%	45.15	1.89	16.46	9.00	0.16	5.82	10.59	3.16	1.76	0.60	0.64	7.8	0.298	0.146	2.05	3.4	875	230
5-21a	79.6	5%	44.12	1.72	15.97	10.77	0.12	6.98	9.83	3.14	1.80	0.49	0.62	7.3	0.267	0.135	1.98	3.1	985	215
5-22	81.2	4%	44.79	1.69	15.79	10.02	0.14	7.18	9.85	3.22	1.77	0.50	0.62	7.9	0.270	0.134	2.01	3.1	760	195
5-30a	82.2	3%	44.47	1.77	16.09	9.70	0.15	6.45	11.17	3.13	1.80	0.60	0.69	9.3	0.296	0.153	1.94	2.8	640	160
5-21b	79.6	5%	43.95	1.80	16.67	10.58	0.20	6.86	10.14	3.36	1.85	0.50	0.61	7.9	0.275	0.138	1.99	2.3	800	150
5-26b	78.5	6%	46.25	1.91	17.41	11.09	0.28	5.89	8.60	4.35	2.65	0.69	0.49	nd	0.171	0.188	0.91	1.2	275	55
5-26a	78.5	6%	47.22	1.96	17.18	10.80	0.26	5.74	7.97	4.41	2.89	0.76	0.46	nd	0.125	0.206	0.61	1.0	275	50
5-1b	80.8	Emb	46.37	1.82	17.69	10.14	0.16	3.80	9.48	4.40	2.65	0.68	0.54	nd	0.141	0.187	0.76	1.3	230	50
5-15a	79.1	Emb	47.84	1.88	18.06	9.37	0.21	3.52	9.02	4.84	2.77	0.60	0.50	nd	0.140	0.200	0.70	0.7	300	50
5-19	79.2	Emb	49.12	2.17	17.12	9.77	0.20	3.56	9.25	4.26	2.98	0.74	0.54	nd	0.142	0.205	0.69	1.2	210	45
	-	Matrix	50.04	2.06	16.22	10.48	0.23	3.23	7.43	4.41	3.5	1.04	0.46	nd	0.010	0.190	0.05	0.1	MDL	-
11 November (ET02-15)																				
15-1a	81.1	2%	45.32	1.76	16.27	9.16	0.19	5.62	11.68	3.41	1.99	0.56	0.72	8.8	0.319	0.159	2.01	2.6	1100	196
15-6a	80.9	3%	44.94	1.77	16.57	9.30	0.15	5.65	11.73	3.39	1.96	0.60	0.71	8.9	0.338	0.167	2.02	2.6	970	187
15-1e	81.1	1%	45.59	1.84	16.95	9.09	0.15	5.59	11.65	3.33	2.04	0.56	0.69	9.5	0.325	0.168	1.94	2.2	1165	185
15-6b	80.9	1%	45.68	1.98	16.65	9.13	0.22	5.52	10.97	3.49	1.98	0.59	0.66	9.6	0.303	0.163	1.86	2.3	1000	174
21 November (ET02-24)																				
24-10a	81.9	4%	45.47	1.79	16.54	9.18	0.17	6.00	11.59	3.32	2.02	0.58	0.70	9.6	0.329	0.168	1.96	2.9	1910	300
24-1	80.6	0%	44.80	1.82	16.58	8.59	0.16	5.16	12.11	3.55	2.08	0.58	0.73	9.3	0.347	0.174	2.00	2.7	1760	275
24-34a	82.3	3%	43.68	1.87	16.34	9.29	0.14	6.22	11.48	3.25	2.04	0.60	0.70	8.5	0.327	0.162	2.02	2.6	1735	265
24-23a	80.7	1%	45.08	1.99	17.74	8.83	0.17	5.29	10.61	3.82	1.93	0.66	0.60	8.5	0.279	0.148	1.89	3.0	1530	265
24-17a	81.7	3%	44.96	1.84	16.43	9.25	0.15	5.95	11.18	3.34	2.00	0.57	0.68	8.8	0.318	0.141	2.25	2.8	1210	220
24-28b	81.3	5%	43.26	2.15	15.99	10.77	0.28	6.77	12.15	3.07	1.86	0.59	0.76	8.3	0.308	0.135	2.27	2.4	1340	210

Table 2. (continued)

Sample[a]	Fo,[b] mol %	PEC[c]	SiO_2, wt %	TiO_2, wt %	Al_2O_3, wt %	FeO,[d] wt %	MnO, wt %	MgO, wt %	CaO, wt %	Na_2O, wt %	K_2O, wt %	P_2O_5, wt %	CaO /Al_2O_3	B, ppm	S, wt %	Cl, wt %	S/Cl	H_2O, wt %	CO_2,[e] ppm	P,[f] MPa
24-7b	81.6	2%	45.20	1.75	16.25	9.18	0.19	5.87	11.60	3.36	1.98	0.59	0.71	9.1	0.318	0.165	1.93	2.7	1145	210
24-7a	81.6	5%	45.49	1.79	16.20	9.18	0.12	5.92	11.75	3.37	1.98	0.55	0.73	8.7	0.299	0.156	1.91	2.7	1175	210
24-41	81.1	4%	44.15	1.84	16.11	10.37	0.18	6.42	11.41	3.11	2.07	0.56	0.71	8.4	0.324	0.157	2.07	2.4	1120	190
24-9	81.5	3%	45.54	1.88	16.77	9.24	0.08	5.85	11.57	3.26	2.05	0.58	0.69	9.4	0.324	0.167	1.95	2.6	1000	185
24-28a	81.3	3%	44.02	2.04	16.26	10.14	0.17	6.31	11.78	3.22	2.01	0.60	0.72	8.7	0.315	0.160	1.97	2.3	1065	180
24-8	81.5	2%	44.30	1.87	16.82	9.36	0.20	5.92	11.60	3.51	2.13	0.59	0.69	9.0	0.324	0.183	1.78	2.2	1075	175
24-29b	75.6	0%	45.56	1.52	17.44	10.30	0.19	4.57	9.57	3.90	1.75	nd	0.55	9.0	nd	nd	nd	2.6	875	175
24-28c	81.3	4%	44.54	2.03	15.94	10.29	0.16	6.46	11.71	3.22	1.92	0.60	0.73	9.0	0.312	0.157	1.99	2.2	1055	175
24-33a	79.7	1%	44.56	1.74	16.98	9.94	0.17	5.59	10.51	3.30	1.87	0.58	0.62	8.0	0.296	0.147	2.02	2.7	565	145
24-22b	81.4	Emb	48.23	1.82	17.96	10.23	0.23	3.60	8.56	4.87	2.81	0.69	0.48	nd	0.122	0.187	0.65	1.1	250	50
24-15	79.5	Emb	48.29	1.68	17.62	9.51	0.18	3.77	9.47	4.19	2.81	0.60	0.54	nd	0.162	0.175	0.93	1.1	200	45
24-27b	81.7	Emb	47.05	1.79	17.60	9.83	0.24	3.95	9.58	4.84	2.53	0.69	0.54	nd	0.198	0.183	1.08	1.2	190	45
24-34b	82.6	Emb	46.70	1.78	18.19	9.92	0.22	3.77	9.94	4.90	2.41	0.71	0.55	nd	0.191	0.190	1.00	0.4	220	35
24-29a	75.6	3%	48.66	2.09	16.57	10.23	0.26	4.56	8.18	4.78	3.20	0.82	0.49	nd	0.088	0.210	0.42	0.5	220	35
24-22a	81.4	Emb	50.71	2.07	16.45	10.28	0.18	3.06	7.15	4.94	3.48	0.99	0.43	nd	0.013	0.213	0.06	0.4	200	30
	-	Matrix	50.09	2.15	15.1	10.79	0.23	3.1	7.19	4.24	3.5	0.94	0.48	nd	0.010	0.240	0.04	0.1	MDL	-
	-	Matrix	49.77	2.15	15.6	10.55	0.21	3.11	7.08	4.53	3.46	1.04	0.45	nd	0.010	0.230	0.04	0.2	MDL	-
									9 December (ET02-35)											
35-30a	81.7	3%	44.78	1.77	15.10	9.95	0.19	6.39	11.61	3.00	1.72	0.52	0.77	8.4	0.289	0.154	1.87	3.2	3145	425
35-30b	81.7	3%	44.83	1.72	15.15	10.11	0.18	6.47	11.61	2.87	1.77	0.52	0.77	8.4	0.294	0.160	1.83	3.1	1475	265
35-16	80.0	3%	45.49	1.64	15.92	9.91	0.17	5.72	11.26	3.09	2.00	0.55	0.71	8.8	0.314	0.162	1.93	2.8	1145	215
35-15	81.2	3%	45.05	1.75	16.32	9.35	0.15	5.79	11.86	3.16	1.88	0.59	0.73	9.3	0.316	0.165	1.92	2.7	1130	210
35-18	76.6	0%	45.21	1.44	17.27	10.47	0.25	5.02	10.56	3.26	1.92	0.54	0.61	8.3	0.334	0.162	2.06	2.7	1100	205
35-10	81.3	0%	45.66	1.75	16.78	8.77	0.14	5.64	11.32	3.47	2.19	0.62	0.68	9.2	0.330	0.159	2.08	2.8	1025	205
35-6	80.0	4%	45.42	1.74	16.12	9.73	0.19	5.64	11.88	3.28	1.86	0.61	0.74	9.4	0.299	0.161	1.86	2.4	1030	195
35-9	81.7	3%	45.09	1.76	15.94	9.53	0.14	6.13	11.53	3.21	2.03	0.61	0.72	8.0	0.308	0.155	1.98	2.2	860	150
35-1	81.5	3%	45.44	1.73	15.87	9.49	0.14	6.04	11.42	3.14	1.99	0.58	0.72	9.1	0.314	0.162	1.94	2.7	515	140
35-31a	74.8	3%	49.26	1.82	17.55	9.50	0.16	4.10	8.61	4.30	2.95	0.63	0.49	nd	0.048	0.213	0.23	0.3	150	25
35-12a	82.3	Emb	48.74	1.66	18.14	9.44	0.22	3.48	9.09	4.41	3.09	0.68	0.50	nd	0.114	0.200	0.57	0.6	140	25

[a]When more than one melt inclusion has been analyzed in a single phenocryst, letters following the number are to distinguish each inclusion or glass embayment.
[b]Fosterite content of host olivine, Fo = [100 × Mg/(Fe + Mg)].
[c]PEC, extent of postentrapment olivine crystallization used to correct the melt inclusion composition. PEC was not applied to glass embayments.
[d]All iron calculated as FeO.
[e]Except for ET02-35 31 and ET02-35 12, CO_2 values are more than 3 times higher than detection limit and thus significant.
[f]Total pressure of melt entrapment was computed from H_2O and CO_2 contents using $V_{OLATILE}C_{ALC}$ program [*Newman and Lowenstern*, 2002]; Emb, glass embayment; nd, not determined; MDL: minimum detection limit.

from the lower vents of the 2001 flank eruption and from lava fountains that happened at SEC in May–June 2000 and June–July 2001 (Figures 3c and 3d). However, the temporal variations of MgO and trace elements in the 2002 bulk products allow us to identify two eruptive pulses of a more primitive, truly basaltic magma. The main one occurred during the first days of the eruption. It is well characterized by our 29 October samples which have a higher MgO content (7.1 wt %), CaO/Al_2O_3 ratio (0.74) and lower Th, La, Nb contents than all other analyzed products (Figures 3a–3d). This initial pulse of primitive basalt is also recorded in MgO-richer (up to 8.2 wt % (R. A. Corsaro, personal communication, 2005)) bulk lavas erupted on 30 October [*Andronico et al.*, 2005] and 2 November [*Clocchiatti et al.*, 2004]. A second, though more discrete pulse of primitive magma is recorded by our November 21 sample. This latter is richer in MgO (7.5 wt %), has a higher CaO/Al_2O_3 ratio (0.75), and is poorer in both Th (6 ppm) and Nb (34.8 ppm) than all products erupted previously (since mid-November) and subsequently (Figures 3a–3d). Its high CaO/Al_2O_3 ratio and low trace element content discard the possibility that its high MgO content could result from a cumulative effect of olivine crystals. Its extrusion actually preceded a threefold peak increase in both the SO_2 output (Figure 2b) and the S/Cl ratio of eruptive gas emissions on 24 November [*Andronico et al.*, 2005].

[21] Starting from the chemical composition of this primitive basaltic magma (7.1 wt % MgO), we used the MELTS software [*Ghiorso and Sack*, 1995] to simulate its conditions of differentiation. Crystal fractionation was modeled for initial pressures of 300 and 200 MPa, a temperature varying from 1160°C (liquidus temperature) to 1125°C, redox conditions close to the NNO buffer [*Métrich and Clocchiatti*, 1996], and for a variable H_2O content. Water concentrations and pressures are constrained from our data for melt inclusions, as described in subsequent sections. The compositional range of bulk erupted lavas, with CaO/Al_2O_3 varying from 0.74 to 0.61 (Figure 4), can be accounted for by the removal of on average 12% clinopyroxene and olivine (in proportions 11:1) from the basaltic melt containing 2.1 wt % H_2O, at between 1150 and 1135°C and 200 MPa. At 300 MPa, with 3 wt % of dissolved water, the amount of crystallization is minor (6–7.5%) and the computed proportions of clinopyroxene and olivine (5:1 at 1140°C to 6:1.5 at 1130°C) result in a more limited decrease of CaO/Al_2O_3 ratio from 0.74 to 0.68.

4.2. Olivine-Hosted Melt Inclusions and Glass Embayments

[22] In all scoriae and lapilli samples the predominant olivines are euhedral microphenocrysts (0.5–1 mm) that range in composition from $Fo_{82.5}$ to $Fo_{79.0}$, exceptionally Fo_{84} in one sample (9 December). These crystals are homogeneous, with a thin rim whose forsterite content is lower by only 0.5 to 2 mol %. However, we also encountered some Fe-richer (Fo_{74} to Fo_{79}) and reversely zoned olivine crystals, especially in the 27–28 October and 21 November samples.

[23] Most olivine crystals have trapped melt inclusions which vary in size from 40 to 200 μm and contain a bubble of variable dimension. We estimated the bubble volume fraction in each melt inclusion (V_B/V_{MI}) by assuming a spherical and a parallelepipedic shape for the bubble and the inclusion, respectively. The values fall between ~0.04 and 0.08 in most inclusions (Figures 5a and 5b) but can reach 0.10 to 0.20 in a few of them (Figure 5c). In particular, some olivine crystals contain inclusions with variable V_B/V_{MI} ratio (Figure 5d) and with typical necking down features (Figure 5e), which is indicative of heterogeneous gas/melt trapping [*Roedder*, 1984]. The potential influence of bubble size upon the dissolved CO_2 content of the inclusions is examined later. Finally, during magma ascent some olivine crystals also trapped melts under the form of glass embayments (Figure 5f) that are either isolated or still connected with the surroundings. These embayments witness a stage of rapid crystal growth, preventing the typical enclosure of a truly isolated inclusion.

[24] The extent of postentrapment olivine crystallization (PEC%) on the walls of each inclusion upon cooling was calculated assuming olivine–liquid equilibrium and using a K_D $[(FeO/MgO)_{olivine}/(FeO/MgO)_{melt})]$ of 0.30–0.29, according to *Métrich and Clocchiatti* [1996]. Iron diffusion from inclusion to olivine is unlikely since the Fe concentration of the melt inclusion is closely similar to that of the corresponding bulk lava. The computed PEC values are low (generally <4%) and introduce only a small correction on measured compositions. Table 2 reports the corrected contents of major oxides, trace elements and dissolved volatiles in all inclusions in which H_2O and CO_2 could be measured systematically.

4.2.1. Phase I

[25] The initial stage of the eruption, corresponding to the main pulse of primitive magma, is represented by our 27 to 29 October samples (ET02-7, ET02-8, and ET02-5). In each sample, the compositional range of melt inclusions trapped in olivines $Fo_{82.5\text{-}79.5}$ overlaps that of the bulk rocks (CaO/Al_2O_3 = 0.73–0.61; K_2O = 1.7–2.1 wt %; Figure 4). Their content in boron (7.3–8.9 ppm), sulphur (0.27–0.33 wt %; Figure 6a) and chlorine (0.13–0.17 wt %; Figure 6b) covaries with K_2O, defining constant K_2O/B (2300 ± 200) and Cl/K_2O (0.08 ± 0.01). The slight decrease of S/K_2O ratio (from ~0.18 to 0.15) as potassium increases raises the possibility of a minor exsolution of S as differentiation progresses, despite the 6% relative error on this ratio. However, this variation is hardly reflected in the S/Cl ratio (2 ± 0.2; Figure 6c), given the analytical uncertainties.

[26] The most primitive inclusions contain ~4 wt % of total dissolved volatiles, including 3.4 ± 0.2 wt % H_2O on average (Figure 7a). Water soon decreases (to 3.1 wt %) with increasing K_2O (Figure 7b). Their CO_2 content is much more variable, from 2795 to 630 ppm (Figure 7c), and shows no systematic relationship with the estimated V_B/V_{MI} ratio. As an illustration, the two inclusions shown in Figures 5a and 5d have similar V_B/V_{MI} ratio but widely different CO_2 concentrations of 2795 and 1860 ppm (Table 2). However, we also found some primitive inclusions (1.8–2.0 wt % K_2O, H_2O > 3 wt %) with a large bubble (V_B/V_{MI} ratio >0.10) that are clearly depleted in CO_2 (<1300 ppm, CO_2/H_2O < 0.04). In their case, it is much likely that postentrapment CO_2 diffusion into the bubble reduced the dissolved carbon content of the glass. This is supported by the detection of carbon on the walls of the largest bubbles during nuclear microprobe analysis, but whose total amount could not be quantified. Therefore the

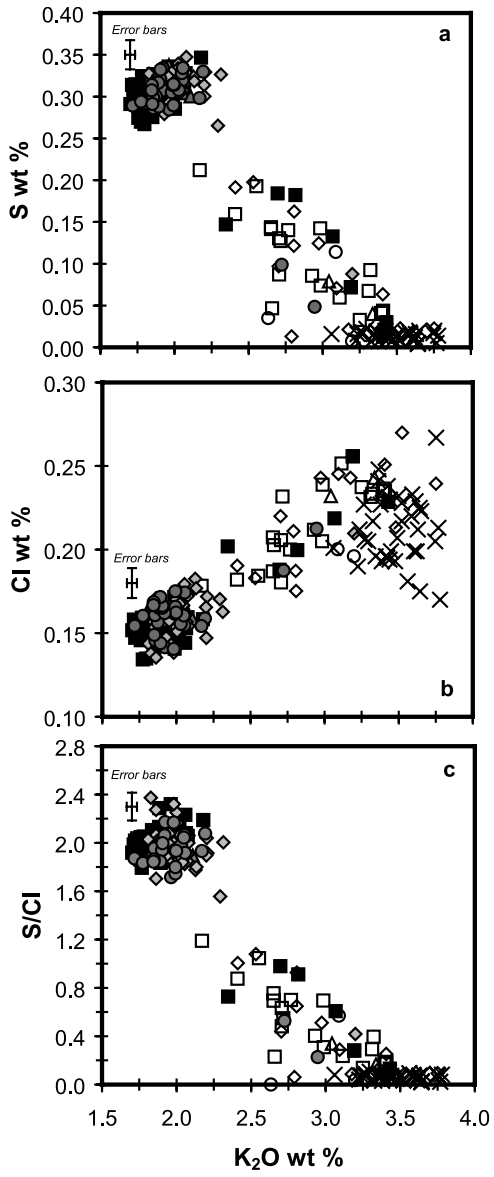

Figure 6. Variability of (a) S and (b) Cl contents versus K_2O and evolution of (c) S/Cl ratio versus K_2O, in melt inclusions, embayments, and matrix glasses from the 2002 samples. Note that both S and Cl increase with K_2O in primitive melt inclusions (K_2O < 2.4 wt %) then exhibit very contrasted behavior along with magma differentiation, as illustrated by the sharp decrease of S/Cl ratio. Symbols are as in Figure 4.

low CO_2 content of these inclusions may not represent a true evolution of the magma and provides entrapment pressure that are underestimated by an unknown amount. Finally, we found in the 27–28 October samples some peculiar primitive melt inclusions that are rich in CO_2 (2330–1240 ppm) but relatively depleted in water (2.7–2.9 wt %), whose significance is addressed in section 5.2.

[27] Compared to the above primitive inclusions, both the glasses embayed in the same olivines ($Fo_{8.1.5-79.5}$) and the melt inclusions trapped in the rare Mg-poorer (Fo_{77-79}) olivines have a more evolved composition (CaO/Al_2O_3 < 0.6, K_2O > 2.4 wt %), sometimes reaching that of the matrix glass (Figure 4). These more evolved glasses are also depleted in S (0.18–0.03 wt %; Figures 6a and 7a), H_2O (1.3–0.3 wt %; Figures 7a and 7b) and CO_2 (385–210 ppm; Figure 7c), but are relatively enriched in Cl (up to 0.26 wt %; Figure 6b). In some olivines, a process of fast decompression and degassing is recorded by weakly evolved (2.4 wt % K_2O) glass embayments which have lost substantial H_2O (0.7 wt %; Figure 7b) and sulphur (0.16 wt %), but no chlorine (0.18 wt %).

[28] Our 11 November scoria sample (ET02-15) characterizes the end of that first phase of the eruption. Its predominant olivines ($Fo_{81.5}$-$Fo_{80.9}$) are similar to those in October samples, but their melt inclusions are slightly more evolved (Figure 4) and are significantly impoverished in volatiles compared to the inclusions in the first erupted

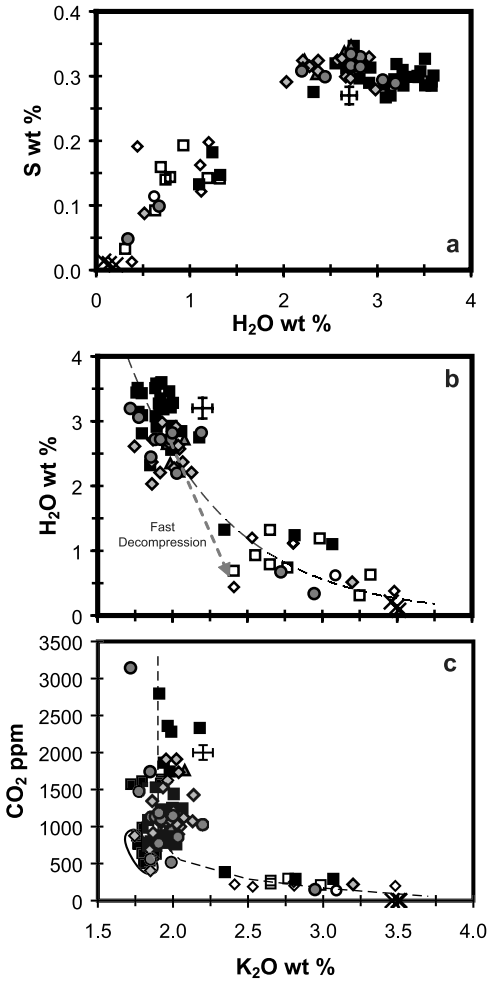

Figure 7. Evolutions (a) of sulphur versus H_2O and of (b) H_2O and (c) CO_2 versus K_2O in melt inclusions, embayments, and matrix glasses from the 2002 eruption. The black contour includes primitive melt inclusions whose bubble volume fraction is ≥0.1, and whose relative CO_2 depletion (<1300 ppm, CO_2/H_2O < 0.04) indicates some postentrapment CO_2 diffusion in bubble. Symbols are as in Figure 4.

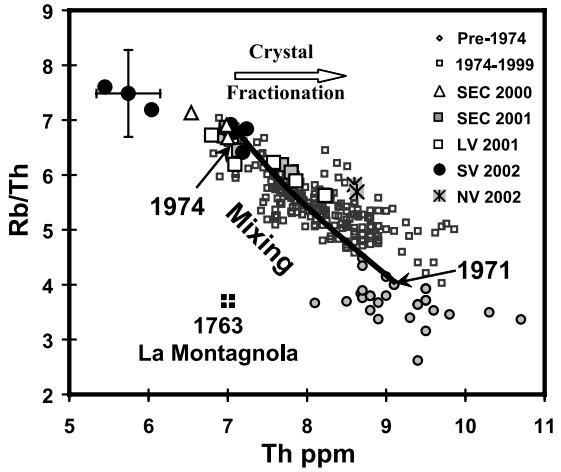

Figure 8. Variations of Rb/Th ratio versus Th in 2002 erupted bulk products [*Clocchiatti et al.*, 2004; this study] compared to pre- and post-1974 Etna lavas. Adapted from *Métrich et al.* [2004] with permission, with addition of products from the 2000 and 2001 lava fountains at SEC crater [*Spilliaert*, 2006]. Crystal fractionation does not affect the Rb/Th ratio, so simple magma differentiation leads to purely horizontal trends (arrow). The chemical evolution of Mount Etna lavas since 1971 is best accounted for by a gradual mixing between the alkali-rich basaltic end-member (Th $\sim$ 7 ppm) erupted in 2000–2002 (and, for the first time, in 1974) and the pre-1974 K-poorer trachybasalts (Th $\sim$ 9.4 ppm) that were previously filling the plumbing system. Rubidium and thorium in 2000–2002 samples were determined with ICP-MS at CRPG (Nancy, France), while with Instrumental Neutron Activation (Laboratoire Pierre Süe, Saclay) in pre-2000 samples [see *Métrich et al.*, 2004, and references therein].

products. They are poorer in H_2O (2.7–2.2 wt %; Figures 7a and 7b) and CO_2 (1165–970 ppm; Figure 7c), while containing as much S (0.30–0.34 wt %) and Cl (0.16–0.17 wt %; Figures 6a and 6b). Glass embayments in the same olivines, as well as melt inclusions in few Mg-poorer crystals ($Fo_{79\text{-}75}$), are still more evolved ($CaO/Al_2O_3 < 0.50$; Figure 4), depleted in S (Figure 6a) and richer in Cl (Figure 6b), as already found in October samples.

4.2.2. Phase II

[29] Our scoriae sample from 21 November (ET02-24) represents a paroxysmal period in the second eruptive phase. As already mentioned, it recorded a discrete new upsurge of the primitive basaltic magma that preceded the highest SO_2 peak emissions in the whole eruption (Figure 2b). This sample is similar to the 29 October primitive basalt in its bulk composition, but also in the CaO/Al_2O_3 (Figure 4), K_2O/B and S/Cl (Figure 6c) ratios of melt inclusions trapped in its Mg-rich ($Fo_{82.5\text{-}79.0}$) olivine crystals. This demonstrates a supply from the same bulk magma. However, the slightly higher contents of K_2O (1.8–2.2 wt %), S (0.28–0.36 wt %; Figure 6a) and Cl (0.14–0.18 wt %; Figure 6b) in its inclusions indicate that the entrapped melt was relatively more evolved than the most primitive melt found in 29 October olivines. In addition, this melt was significantly depleted in water (3.0–2.2 wt %; Figures 7a and 7b) for comparable amounts of CO_2 (from 1910 to 565 ppm; Figure 7c) and thus had a lower bulk volatile content (3–3.5 wt %). Note that we observe no obvious relationship between the CO_2 content and the bubble size of the inclusions. While most inclusions have a typical V_B/V_{MI} ratio of $\sim$0.05 (e.g., Figure 5b), we measured the highest amount of CO_2 in one inclusion with V_B/V_{MI} ratio >0.10. We also found similar CO_2 (1175 and 1145 ppm) and H_2O (2.7 wt %) contents (Table 2) in inclusions with very different V_B/V_{MI} ratio and that were trapped in one single crystal (Figure 5e). These features indicate heterogeneous gas/melt trapping. We thus consider the amounts of CO_2 dissolved in these inclusions to be closely representative of the CO_2 content of the magma at the time of entrapment.

[30] Our sample from 9 December (ET02-35) represents the final stage of the second eruptive phase. While it is typical of the bulk trachybasaltic magma produced by the eruption (Figure 4), its olivine crystals are generally more evolved ($Fo_{72\text{-}75}$), contain Fe-Ti oxides, and their melt inclusions are usually crystallized, which prevents their analysis. However, we also found homogeneous, euhedral olivines $Fo_{82.6.9\text{-}78.9}$ with a majority of melt inclusions that are more primitive ($CaO/Al_2O_3 > 0.69$) than the bulk rock ($CaO/Al_2O_3 = 0.65$, Figure 4) and therefore were not in equilibrium with the carrier lava. These inclusions are identical to those in the 21 November sample in their concentrations of K_2O (1.9–2.2 wt %), B (8.0–9.4 ppm), H_2O (<3.0 wt %, Figures 7a and 7b) and CO_2 (2000–1025 ppm, Figure 7c), but also in their S/Cl (Figure 6c) and V_B/V_{MI} ($\sim$0.04–0.08) ratios. Only one crystal has trapped two inclusions showing covariations in CO_2 (3145 and 1475 ppm, Figure 7c) and V_B/V_{MI} ratio (respectively $\sim$0.02 and 0.08), suggesting some possible postentrapment CO_2 diffusion in the inclusion with larger bubble. However, dynamic entrapment of variably degassed melt cannot be excluded since the CO_2-depleted inclusion has a more elongated shape than the totally spherical CO_2-rich one.

[31] Finally, both 21 November and 9 December samples were found to contain more evolved glasses either trapped as embayments in the most primitive olivines (Fo > 80) or as inclusions in some Fe-richer crystals ($Fo_{79\text{-}75}$; Figure 4). These glasses still contain high amounts of Cl (0.16–0.27 wt %, Figure 6b), but are impoverished in S (0.19–0.02 wt %; Figure 6a), H_2O (1.1–0.4 wt %, Figure 7b), and CO_2 (250–140 ppm, Figure 7c).

4.3. Matrix Glasses

[32] The groundmass of erupted scoriae and lapilli frequently contains microlites that make the analysis of the residual glass delicate. Therefore we specifically selected and prepared vesicular fragments of scoriae from 28–29 October and 21 November for matrix glass analysis. These glasses contain 3.1–3.8 wt % K_2O and represent the most evolved terms of the differentiation trend for the 2002–2003 eruption (Figure 4). Their volatile content is very low: $H_2O < 0.2$ wt %, S < 0.02 wt %, Cl = 0.27–0.18 wt %, while CO_2 is below the detection limit (<55 ppm). With respect to the most primitive inclusions, they demonstrate an extensive ($\geq$95%) loss of water, carbon dioxide and sulphur during magma ascent and eruption. On the contrary, their high Cl content (Figure 6b) and very low S/Cl ratio

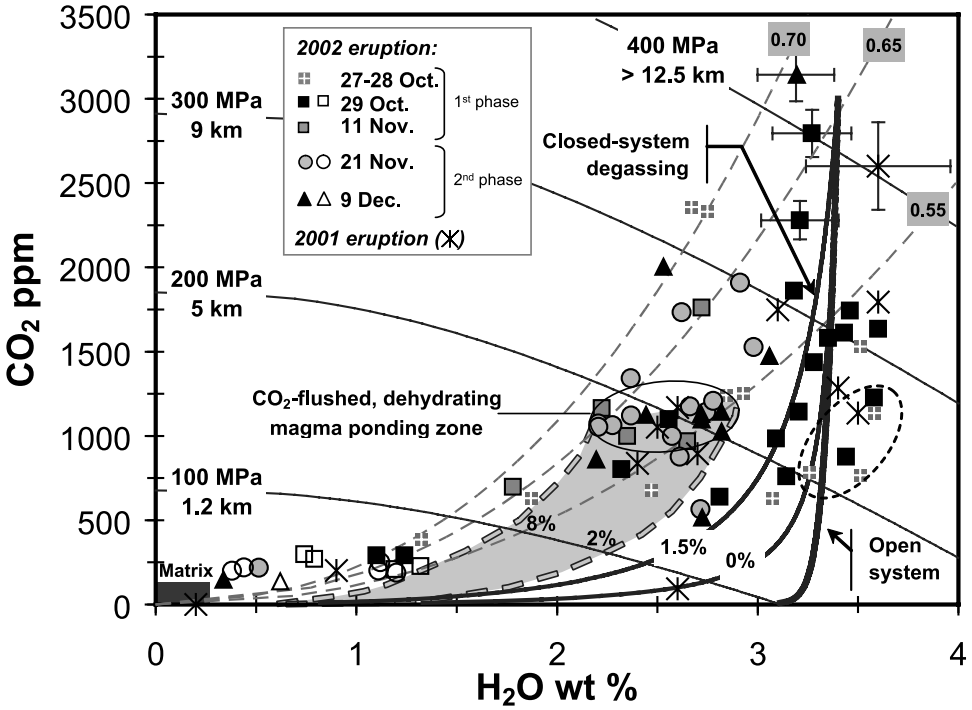

Figure 9. Evolution of CO_2 and H_2O contents of melt inclusions (plain symbols), glass embayments (open symbols) and matrix glasses. Isobars, degassing trends, and curves of equilibrium between the melt and a vapor phase of fixed composition (isopleths) are calculated at 1140°C using $V_{OLATILE}C_{ALC}$ [*Newman and Lowenstern*, 2002]. Lithostatic depths (in km bsl) corresponding to isobars are derived from the density of sedimentary layers forming Etna's basement [*Corsaro and Pompilio*, 2004b]. On each isopleth is indicated the molar fraction of carbon dioxide (X_{CO_2}) in the equilibrium gas phase. Decompression of the primitive basaltic melt containing 3.4 ± 0.2 wt % dissolved H_2O at ~400 MPa is modeled in either open system or closed system with 0 and 1.5 wt % initial gas phase. Most data points for the initial eruption stage (27–29 October) fit with closed system magma degassing with 1.5 wt % initial gas. The few inclusions depleted in CO_2 after trapping (dashed contour; see Figure 6c) depart from this trend. Most of the erupted magma is represented by the cluster of inclusions trapped at between 220 and 170 MPa. These define a magma ponding zone at 5 ± 1 km bsl, affected by deep CO_2 flushing and consequent variable magma dehydration (plain contour). This latter process can also account for a water-depleted inclusions trapped at pressures of ~300 MPa (see text). Finally, melt inclusions and glass embayments trapped between 170 MPa and the surface can only be explained by closed-system ascent and degassing of the magma ponding 5 ± 1 km bsl, in presence of between 2 and ≥8 wt % of gas (grey area). Melt inclusion data for the 2001 flank eruption [*Métrich et al.*, 2004] are shown for comparison.

(<0.1; Figure 6c) point to a maximum loss of 40% of chlorine.

5. Discussion

5.1. Eruption of the Parental Alkali-Rich End-Member of Post-1970s Etna Lava Series

[33] In addition to their unusual explosivity, the 2001 and 2002–2003 flank eruptions of Etna are the first events in the last three centuries to have produced two distinct magma types at the same time. The plagioclase-bearing trachybasalts extruded from the upper vents in 2001 and along the northern flank in 2002 share a very similar chemistry and mineralogy with evolved and partly degassed lavas from the central volcano conduits [*Métrich et al.*, 2004; *Andronico et al.*, 2005; this study]. Their relatively high thorium content and low Rb/Th ratio indicate that these trachybasalts were derived from a shallow crystallizing magma that had previously mixed with alkali-poorer magma belonging to the pre-1970s series (Figure 8). Their simple drainage from the central volcano conduits was demonstrated in 2001 [*Métrich et al.*, 2004; *Clocchiatti et al.*, 2004] and, in 2002, is supported by seismic and geodetic evidence of northward dike propagation from these conduits during the first days of the eruption [*Aloisi et al.*, 2003; *Monaco et al.*, 2005; INGV reports, 2002].

[34] In contrast, the more primitive, plagioclase-poor trachybasalts erupted through the south vents in 2002–2003 clearly drained a deeper portion of the plumbing system and rose through a separated dike, despite its extrusion at only ~1.5 km distance from the summit craters. In particular, its unusual lack of plagioclase phenocryst implies its fast ascent from depth with limited preeruptive loss of water [*Métrich and Rutherford*, 1998]. This magma is very similar in its chemistry and mineralogy to that produced through the lower vents of the 2001 eruption (Figures 3b and 3c), indicating its derivation from the same

parental melt. This chemical similarity even extends to some lapilli and scoriae produced by lava fountains at SEC in May–June 2000 and June–July 2001 (Figures 3c and 3d). Following the interpretation of *Métrich et al.* [2004] and as depicted in Figure 8, we conclude that all these products are representative of the new alkali-rich magma that has started to feed Mount Etna since the early 1970s. Over the last three decades, this new magma has gradually mixed with and replaced the former alkali-poorer trachybasalts emplaced in the plumbing system, leading to the extrusion of progressively more basic and alkali-richer lavas (Figure 8). However, little of it had been directly extruded prior to 2001, and the 2002 flank eruption represents its more voluminous extrusion until now. Furthermore, we demonstrate here that moderate amounts of a still more primitive component of this magma were extruded during the first phase of the 2002 eruption, and much more discretely on 21 November. This component shares a broadly similar Rb/Th ratio (7.4 ± 0.2, Figure 8) with the main coerupted trachybasaltic products, but differs from them in its lower Th content (6 ppm). It is the most primitive magma erupted by Mount Etna since 240 years (La Montagnola eruption, 1763; Figure 8), and may closely represent the parental alkali-rich end-member of the post-1970s Etna lava series.

5.2. Depth of Ascent and Degassing Pattern of the Erupted Magma

[35] Under the assumption of magma volatile saturation, our data for the dissolved amounts of H_2O and CO_2 in melt inclusions and glass embayments allow us to assess the total fluid pressure ($P_{CO_2} + P_{H_2O}$) at the time of melt entrapment and, therefore the corresponding depth of magma ascent and degassing. We used the $V_{OLATILE}C_{ALC}$ program [*Newman and Lowenstern*, 2002] to compute these pressures and to model the degassing behavior of H_2O and CO_2 during basalt decompression and crystallization under both open and closed system conditions (Figure 9). In order to take account of the strong influence of magma composition on the CO_2 solubility, single pressures and isobaric curves were calculated for Etna basalt-trachybasalts whose SiO_2 contents are computed from the Π coefficient defined by *Dixon* [1997] to be 47 wt % ($H_2O > 2$ wt %) and 48 wt % ($H_2O <$ 2 wt %). Recent experiments however show that a high water content strongly enhances the CO_2 solubility, stabilizing carbonate species in basaltic melt at pressure ≥400 MPa [*Botcharnikov et al.*, 2005]. Because $V_{OLATILE}C_{ALC}$ applies to moderately or weakly hydrous basalts in the 0–500 MPa interval, we thus stress that our highest pressure estimates are upper limits.

[36] Melt entrapment depths were calculated from total fluid pressures by considering the different density of lithologies in the crustal basement of Etna [*Corsaro and Pompilio*, 2004b]. Rock densities of 2500 and 2700 kg m^{-3} are respectively representative for the upper 2 km and lower 8 km of the sedimentary basement below sea level. We also considered a uniform rock density of 2800 kg m^{-3} that takes into account that Etnean magmas rise through a huge plutonic body extending vertically from 0 to 18 km beneath the volcano [e.g., *Laigle et al.*, 2000; *Chiarabba et al.*, 2000]. In the pressure range from 0 to 400 MPa, these two calculations yield relatively small differences (7 to 20 MPa, or 300 to 800 m in depth).

[37] The results depicted in Figure 9 show that the analyzed melt inclusions and glass embayments plot along two main distinct trends, implying different conditions of magma ascent and degassing.

[38] The first trend is depicted by the most primitive inclusions in the most mafic products of the eruption, especially those extruded during powerful lava fountains on 29 October. Most of them were trapped at pressures ranging from ∼400 to 200 MPa, indicating the ascent and polybaric entrapment of the primitive basaltic melt from >10 to 5 km depth bsl. In this depth interval, the inclusions define a main trend of basalt decompression and degassing during which CO_2 rapidly exsolves, whereas H_2O remains almost unchanged with respect to its initial average content of 3.4 ± 0.2 wt % (this average value being the most representative taking account of analytical error bars; Figure 9). Despite its apparent fitting, such a trend can hardly be accounted for by open system degassing, for the following reasons: (1) this process cannot explain the volatile-depleted glass embayments and more evolved inclusions that were trapped at low pressure (∼50 MPa) in the same samples, (2) it is physically incompatible with the fast uprise and violent eruption of the corresponding magma, and (3) its apparent fit is strongly determined by water-rich inclusions with low CO_2 content which we already showed to have been affected by posttrapping CO_2 diffusion (dashed contour in Figure 9). Instead, a closed system degassing process, in which the exsolved volatiles remained in contact with the melt, is physically more realistic and better accounts for our data. The two curves labeled 0 and 1.5% in Figure 9 represent closed system degassing of the basalt with zero to 1.5 wt % initial vapor at 400 MPa. The presence of a CO_2-rich gas phase at that pressure is most likely, given the high original CO_2 content of ∼1.5 wt % in Etna primary magma [*Allard*, 1999] inferred from the time-averaged CO_2/S ratio in Etna summit plume emissions. For such an original CO_2 content, the equilibrium vapor phase at 400 MPa contains 1.2 wt % CO_2 and 0.26 wt % H_2O ($X_{CO_2} = 0.65$ by mole). Note that this would imply that Etna primary magma may originally contain ≥3.7 wt % of dissolved water. Closed system decompression of the primitive basalt coexisting with such a vapor phase well explains our data, taking account of the error bars on both H_2O and CO_2. The ascending magma composed of melt + crystals + 1.5 wt % vapor is computed to have a density of ∼2240–1940 kg m^{-3} at 1140°C in the range 400–200 MPa, compared to 2650 kg m^{-3} for the host sedimentary rocks [*Corsaro and Pompilio*, 2004b]. It should thus be strongly buoyant and, given its low viscosity (∼ 0.9 Pa s for the melt at 1140°C [*Giordano and Dingwell*, 2003]), could have risen with a speed high enough to maintain closed system conditions until close to the surface. From $V_{OLATILE}C_{ALC}$ and the amounts of CO_2 and H_2O exsolved upon ascent, we compute a total gas volume fraction reaching ∼77% at 10 MPa, able to promote magma fragmentation and to sustain the powerful lava fountains and ash emissions that marked the initial phase of the eruption.

[39] The second trend in Figure 9 is principally defined by samples from the second eruptive phase and thus refers

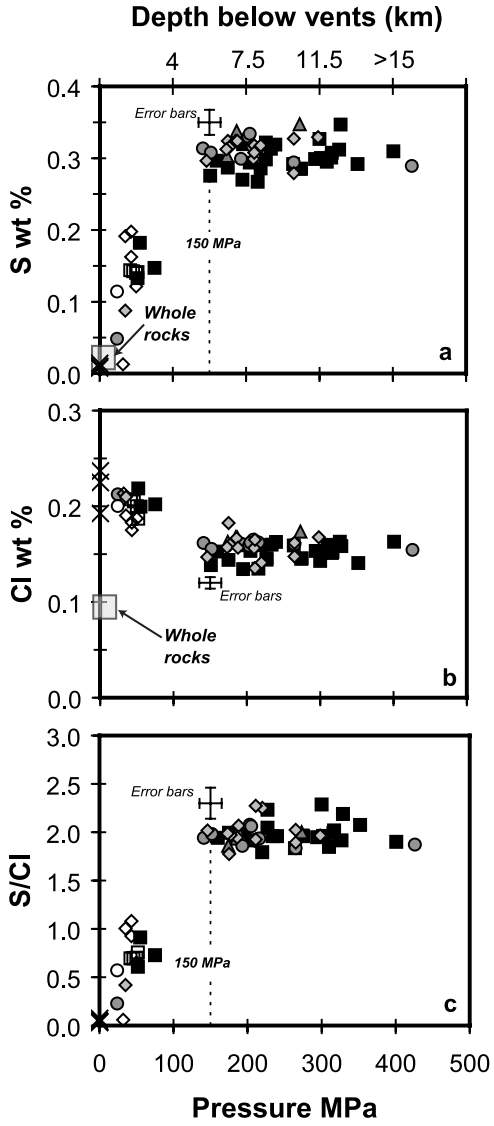

Figure 10. Pressure-related evolutions of (a) S and (b) Cl contents and (c) S/Cl ratio in melt inclusions and matrix glasses from the 2002 eruption. Entrapment pressures and depths are inferred from the dissolved H_2O and CO_2 contents (Table 2 and text). Symbols are as in Figure 4.

to the longest part of the 2002 eruption, even though it also includes a few inclusions from the very beginning (27–28 October) and the end (11 November) of the first phase. Its prominent feature is a cluster of melt inclusions which are slightly more evolved and poorer in water than the 29 October basalt, and whose trapping occurred within a narrow pressure range from 220 to 170 MPa. This clustering indicates a preferential level of magma ponding and crystallization at between 6 and 4 km bsl, which broadly corresponds to the transition between the flyschoid units underlying the volcano and the Hyblean carbonate platform [*Lentini*, 1982; *Bianchi et al.*, 1987; *Chiarabba et al.*, 2000]. Preeruptive magma ponding at such a level was previously inferred from melt inclusions in the 2001 eruption products [*Métrich et al.*, 2004] and from seismic data [e.g., *Murru et al.*, 1999; *Patanè et al.*, 2003]. Moreover, a depth of 5 ± 1 km matches the lower boundary of the 2002 eruption seismicity [e.g., *Aloisi et al.*, 2003; *Gambino et al.*, 2004].

[40] The observed cluster of inclusions delineates a subhorizontal "water depletion" trend where H_2O decreases from 2.9 to 2.2 wt %, while CO_2 weakly varies from 1140 to 1050 ppm. First, such a trend cannot be explained by closed system degassing of the uprising primitive basalt, unless this latter would have coexisted with huge amounts (15 to 20 wt %) of gas at greater depth, which is very unlikely. Second, it cannot be accounted for by equilibrium volatile exsolution in the 220–170 MPa interval, since magma dehydration at constant CO_2 would eventually result in a water-dominated gas phase, in contrast with the theoretical equilibrium gas composition indicated by the isopleths in Figure 9 (X_{CO_2} = 0.65 for 2.2 wt % H_2O). An alternative process could be a mixing between the water-rich primitive melt and magma that has previously been depleted in water during shallow degassing and then drained back. However, this hypothesis is incompatible with the observed lack of reverse zoning of the olivine crystals, the homogenous composition of their melt inclusions and their high sulphur content, which excludes shallow magma degassing (see section 5.3). Therefore the only way to generate selective water depletion in Etna basalt at high pressure and to reconcile these observations is a reequilibration of the magma with a deeper-derived CO_2-rich gas phase. Flushing of the magma by deeper-derived CO_2-rich bubbles (X_{CO_2} from 0.55 to 0.65) during its ponding and crystallization at 5 ± 1 km depth bsl can well explain the selective dehydration recorded by the melt inclusions clustering at around 200 MPa. In order to buffer a gas phase with 65 mol % of CO_2 in equilibrium with the melt inclusions, we compute that either 5 wt % of pure CO_2 or ≥8 wt % of a H_2O-CO_2 mixture with ≤0.85 mol % CO_2 should have been added to the ponding magma.

[41] Deep CO_2 flushing can also account for the CO_2-H_2O content of other few inclusions that were entrapped at higher pressures of 300 ± 30 MPa. The corresponding depth of ~9 ± 1 km depth bsl (Figure 9) coincides with the transition between the Hyblean carbonate series and the underlying crystalline crust [*Lentini*, 1982; *Murru et al.*, 1999], where another magma ponding zone may exist. Continuous CO_2 flushing of Etna plumbing system is consistent with the high original CO_2 content and early saturation of Etna alkali basalt [*Allard et al.*, 1991], as well as with the huge emissions of magma-derived CO_2 from the volcano, even during quiescent periods [e.g., *Allard et al.*, 1991, 1997]. Early CO_2-melt separation may thus be a common process on Etna, except in the case of very fast magma uprise that allows closed system ascent of bubble-melt mixtures, such as concluded for the 29 October lava fountains. Moreover, external carbon dioxide could also be added from the heated Hyblean carbonate basement [*Allard et al.*, 1991], enhancing the CO_2-flushing mechanism. Such a contribution would increase magma dehydration and, as a consequence, would imply a still higher water content in Etna primary magma. Ion microprobe determinations of the D/H isotopic ratio of melt inclusions, currently in progress, should allow us to better quantify the impact of deep CO_2 flushing upon the H_2O content of Etna basalts. In addition to this process, we cannot discard that local mixing events between magma blobs or bubbles containing slightly dif-

Table 3. Gas Yield From the Trachybasaltic Magma Erupted at the 2002–2003 South Vents

	Volcanics, m^3	Magma,[a] kg DRE	H_2O, kg	CO_2, kg	SO_2,[b] kg	HCl, kg
Initial content/kg magma			2.6×10^{-2}	1.5×10^{-2}	6.3×10^{-3}	1.6×10^{-3}
Residual content/kg magma			2.0×10^{-3}	5.0×10^{-5}	1.0×10^{-4}	1.7×10^{-3}
Degassed mass fraction[b]			2.5×10^{-2}	1.5×10^{-2}	6.3×10^{-3}	7.0×10^{-4}
Lava flows	2×10^7	4.2×10^{10}	1.1×10^9	6.4×10^8	2.6×10^8	2.8×10^7
Tephra	4×10^7	5.3×10^{10}	1.3×10^9	7.9×10^8	3.3×10^8	3.5×10^7
Pyroclastic cones	1×10^7	1.6×10^{10}	4.0×10^8	2.4×10^8	1.0×10^8	1.1×10^7
Total		1.1×10^{11}	2.8×10^9	1.7×10^9	6.9×10^8	7.4×10^7

[a]Dense rock equivalent (DRE) magma amounts derived from erupted volumes corrected for their mean vesicularity (lava flows 20%; pyroclastites ~45%) and a solidified basalt density of 2650 kg m^{-3}. Lava flow and tephra volumes from *Andronico et al.* [2005]; volumes of 2750 and 2800 m pyroclastic cones estimated in this study.

[b]The degassed fraction of each volatile from the dominantly erupted trachybasaltic magma is the difference between its pre-eruption and residual content, taking account of 44% crystallization of residual glasses (K_2O increase from ~2.0 to 3.6 wt %; see text). SO_2 contents in magma are elemental S contents multiplied by the SO_2/S molar weight ratio.

ferent amounts of water could have contributed to the range in H_2O exhibited by the inclusion cluster at ~200 MPa.

[42] Finally, magma ascent and degassing between the 6–4 km deep ponding zone and the surface during the eruption is recorded by glass embayments and melt inclusions that were trapped at pressures ranging from 150 down to 50–25 MPa. Closed system magma ascent in presence of between 2 and 8 wt % of gas (grey area; Figure 9) can account for most of them. Several inclusions however preserved significantly more CO_2 (≥210 ppm; Table 2) than expected from this evolution. This suggests an even greater amount of CO_2-rich gas coexisting with the magma at depth, thereby enhancing the idea that deep CO_2 flushing commonly affects the shallow plumbing system of Etna.

5.3. Pressure-Related Degassing Pattern of S and Cl

[43] The pressure-related evolutions of S, Cl and S/Cl ratio in our samples are depicted in Figures 10a–10c. Entrapment pressures are inferred from the coexisting H_2O and CO_2 contents, as described above. We observe a broad constancy of both S and Cl contents and S/Cl ratio (~2) in melt inclusions until 150 MPa. Note, however, that the slight decrease of the S/K_2O ratio along with melt evolution in the primitive inclusions (section 4.2.1) suggests a possible onset of minor sulphur exsolution prior to 150 MPa. Therefore we can just say that little sulphur but no chlorine are exsolved until the magma reaches about 5.5 km depth below the vent or ~3 km bsl. This depth is an upper limit since we found no inclusion trapped in the 150–80 MPa interval and because both the S content and S/Cl ratio of the melt are already reduced by a factor of 2 at 80 MPa. The continued decrease of both parameters afterward (Figures 10a and 10c) evidences a main control of sulphur degassing upon the S/Cl evolution. In fact, almost all sulphur, whereas only 40% at most of chlorine are lost at low pressure and upon eruption, as shown by the high residual amounts of Cl in evolved inclusions, glass embayments and matrix glasses (Figure 10b). Hence our data clearly demonstrate that (1) sulphur degassing beneath Etna becomes significant only in the upper part of the plumbing system, which is an essential information to interpret SO_2 flux changes at the surface and (2) as already shown by data for the 2001 eruption [*Métrich et al.*, 2004], sulphur exsolves earlier and much more extensively than chlorine during Etna basalt ascent, in contrast to previous interpretations [e.g., *Pennisi and Le Cloarec*, 1998; *Aiuppa et al.*, 2002].

[44] In this framework, the gas phase coexisting with the uprising basalt will evolve from a high S/Cl ratio at high pressure (≤150 MPa) down to a low ratio at low pressure. Given the initial and residual contents of S and Cl in the trachybasaltic magma that mainly sustained the 2002 eruption (see section 5.4 and Table 3), a S/Cl weight ratio of ~5 is expected in the erupting gas phase produced by closed-system bulk degassing, whereas any previous gas-melt separation will result in a higher S/Cl ratio [*Burton et al.*, 2003a; *Allard et al.*, 2005; N. Spilliaert et al., S-Cl-F degassing pattern of water-rich alkali basalt: modelling and relationship with eruption styles on Mount Etna volcano, submitted to *Earth and Planetary Sciences Letters*, 2006]. A mean S/Cl weight ratio of 4.5 (range 3.5–5.5) was actually measured with FTIR spectroscopy during the course of the eruption [*Burton et al.*, 2003b; *Andronico et al.*, 2005]. Such a value is typical for syneruptive bulk magma degassing and thus supports our interpretation of prevalently closed-system magma ascent and eruption based on CO_2-H_2O data (Figure 9). Instead, the gradual increase of S/Cl weight ratio from 3.5 to 17 in gases emitted between 18 and 24 November 2002 [*Burton et al.*, 2003b; *Andronico et al.*, 2005] implies a gas/melt separation occurring at increasing depth in the feeder dike in that interval. Therefore, even though the magma erupted dominantly under closed system conditions, these latter data indicate temporary transitions to open system degassing.

5.4. Volatile Budget of the 2002–2003 Eruption

[45] Knowing the respective amounts of volatiles and magma produced by the 2002–2003 eruption can provide additional constraints upon its dynamics and origin. COSPEC measurements indicate a cumulated bulk SO_2 output of $\sim 8.6 \times 10^8$ kg from the volcano during the 94 days of the eruption [*Caltabiano et al.*, 2003], which is equivalent to ~6% of the annual yield by global volcanism [*Andres and Kasgnoc*, 1998]. This bulk SO_2 output includes emissions from the south eruptive vents, but also from the summit craters and, to a lesser extent, the short-lived eruption on the North flank [*Caltabiano et al.*, 2003].

[46] Our results allow us to compute the quantities of SO_2 and other volatiles that were produced by the trachybasaltic

magma dominantly erupted from the south vents and then to compare these quantities with COSPEC data. The degassed mass fraction of each volatile species is given by the difference between its dissolved content in the primitive melt inclusions representative of this magma that was ponding at about 200 MPa and its residual content in the most degassed matrix glasses, corrected for crystallization. The mean increase of potassium from 2.0 wt % in primitive inclusions representative of the erupted magma to about 3.6 wt % in the matrix glasses points to 44% bulk crystallization of the melt, as both phenocrysts and microlites, during ascent and eruption. The primitive inclusions provide accurate figures for the preeruption content of H_2O, S and Cl, but not for CO_2 which starts to exsolve at much greater depth (Figure 9). Following the same reasoning as in section 5.2, we thus considered $\sim$1.5 wt % CO_2 in the undegassed magma [*Allard*, 1999]. The results are given in Table 3.

[47] Syneruptive degassing of magma extruded through the south vents could have released 5.2×10^9 kg of gas, including 2.8×10^9 kg of H_2O, 1.7×10^9 kg of CO_2, 6.9×10^8 kg of SO_2 and 7.4×10^7 kg of HCl. We find that the computed budget for SO_2 represents 80% of the COSPEC-derived total emissions. This is fairly consistent with the proportion occasionally measured with COSPEC when the south eruptive emissions could be distinguished from the summit plume [*Caltabiano et al.*, 2003]. If, moreover, one considers the uncertainties on both the erupted solid volumes (±50% [*Andronico et al.*, 2005]) and COSPEC data (±20–25%), both numbers are found to be very close. This implies little or no excess release of sulphur dioxide during the eruption. Therefore we can conclude that (1) there was no detectable SO_2 accumulation in the shallow ($\leq$3 km depth bsl, section 5.3) plumbing system prior to the eruption, even though the SO_2 discharge from Etna was strongly reduced since the 2001 eruption [*Caltabiano et al.*, 2003], and (2) SO_2 emissions from the south vents were essentially supplied by syneruptive bulk degassing of the extruded magma, in agreement with our interpretation of CO_2-H_2O data (Figure 9).

5.5. Triggering Mechanism of the 2002–2003 Flank Eruption

[48] As previously mentioned, two opposite triggering mechanisms have been advocated for the 2002–2003 eruption on basis of geophysical and volcanological observations. *Acocella et al.* [2003] and *Neri et al.* [2005] proposed that the eruption resulted from magma depressurization as a consequence of eastward flank slip of the volcano, whose evidence includes seismic swarms and ground deformations that occurred since 22 September 2002 along the Pernicana transcurrent fault and on the lower eastern flank of the volcano. In contrast, based on seismic data, *Aloisi et al.* [2003] and *Gambino et al.* [2004] link the eruption to an early intrusion of deep ($\geq$10 km bsl) magma that overpressurized the shallow plumbing system and subsequently triggered dike fracturing and fast magma ascent. The strains caused by this overpressure would have been released away from the summit region, as already observed in other flank eruptions [*Bonaccorso*, 2001], promoting ground movements along the WNW-SSE, NE-SW and Pernicana fault systems, but also fracturing of the central conduits and northward dike propagation.

[49] Our results for the products erupted at the south vents provide further constraints upon the triggering mechanism of the 2002–2003 eruption, especially when considering both its similarities and differences with respect to the precedent 2001 flank eruption. Several lines of evidence demonstrate a close genetic relationship between the two events: (1) their successive occurrence within a short time span and in the same area, (2) the comparable chemistry and mineralogy of their alkali-rich bulk trachybasalts, which in addition carried out uncommon quartz arenite crustal xenoliths, and (3) the comparable depths of preeruptive ponding of their magma. All these aspects actually suggest that the 2002 eruption can be considered a second, longer stage of the 2001 event.

[50] However, the two eruptions also differed in some aspects. First, the magma erupted in 2002 could rise through fractures already opened in 2001 [*Acocella and Neri*, 2003], which were seen to enlarge three weeks before the eruption onset (P. Allard and D. Andronico, unpublished observations, 2002). This explains the much shorter preeruptive seismic crisis (3–4 hours) in 2002 than in 2001 (4 days), but also the lack of olivine xenocrysts mechanically extracted from the volcanic pile in the 2002 products, whereas these latter were abundant in 2001 [*Métrich et al.*, 2004]. There was a minimal erosion of opened conduit walls during magma ascent in 2002, whereas in 2001 the dike intrusion had to force its path across the volcano south flank. Second, the 2002 eruption produced an even more primitive alkali-rich magma than the 2001 event which, furthermore, was principally extruded during the initial phase. Rather, the most primitive terms in 2001 were produced during the final stages of fountaining and Strombolian activity.

[51] It has been shown that the 2001 eruption was triggered by overpressuring of the shallow plumbing system of Etna in response to a deep magma injection in the previous months [e.g., *Patanè et al.*, 2003; *Acocella and Neri*, 2003; *Métrich et al.*, 2004]. Magma overpressuring prior to the 2002 eruption is also supported by the following features. First, geophysical data, in particular, the intense swarm of microseismicity (from 16 to 0 km) that was recorded two months prior to the eruption [*Gambino et al.*, 2004], provided evidence of a precursory deep magma input. Note that the observed gaps between the seismogenic volumes activated at that time (Figure 11) coincide fairly well with the depths of ascent of the primitive basaltic magma ($\geq$10 km bsl) and the bulk trachybasalt (6–4 km bsl) constrained by our melt inclusion data. These depths also match two main transitions between geological units in the crustal basement, where magmas may temporarily reside and crystallize due to neutral buoyancy (Figure 11). Second, the fast (closed system) uprise and extrusion of the most primitive magma from $\geq$10 km depth at the beginning of the 2002 eruption can hardly result from simple decompression of the shallow plumbing system. Instead, it points to a deep magma pulse that, for still unknown geometric reasons (separated drain?), could reach the surface without interacting directly with the slightly more evolved magma body that was emplaced at $\sim$5 km depth bsl and subsequently drained out. Hence magma overpressure was likely the main triggering mechanism of the 2002 eruption, even though its sudden

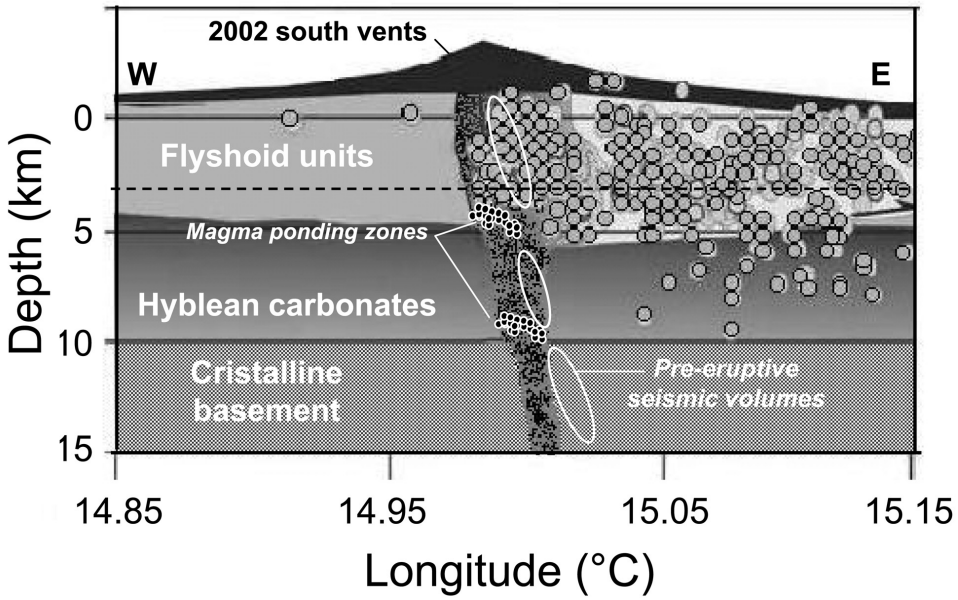

Figure 11. A 2-D schematic representation of Mount Etna plumbing system showing the two magma ponding zones inferred from our crystal melt inclusion data for the 2002 eruption and their relationships with (1) preeruptive (31 August to 3 September 2002) microseismic activity (white contours [*Gambino et al.*, 2004]), (2) 0–5 km deep syneruptive seismicity linked to northeastward dike propagation during the eruption (grey circles [*Neri et al.*, 2005]), and (3) the stratigraphy of the crustal basement (modified from *Neri et al.* [2005], with additions from other sources [*Lentini*, 1982; *Chiarabba et al.*, 2000]). The dashed line marks the possible shallower limit of the transition between the flyschoid series (Maghrebian-Appenninic chain) and the Mesozoic Hyblean carbonates [*Chiarabba et al.*, 2000]. Also drawn schematically is the wide, high-density plutonic body (marbled area) that extends from 0 to 18 km bsl beneath the volcano [*Laigle et al.*, 2000; *Chiarabba et al.*, 2000], around which most earthquakes are distributed [*Patanè et al.*, 2003]. Note the fairly good depth correspondence between the inferred magma ponding zones and the gaps between the seismogenic volumes that were activated at −15 to +1 km depth just 2 months before the eruption. These volumes define the main pathway for magma ascent beneath Etna, along a ∼N-S plane dipping eastward with approximate angle of 70° [*Gambino et al.*, 2004].

onset was facilitated by already opened fractures and eastward flank spreading consecutive to dike intrusion in 2001 [*Neri et al.*, 2005]. The decompression associated with these ground deformations could help explain the four times longer duration of the 2002 eruption compared to the 2001 one. Therefore it is reasonable to conclude that this eruption resulted from a subtle interplay between magma overpressuring and structural depressurization of the shallow plumbing system.

[52] Finally, the uncommon quartz arenite xenoliths present in both 2001 and 2002 south vent lavas provide evidence of mechanical interactions of the uprising magma with the crustal basement. It was suggested [*Monaco et al.*, 2005] that these crustal xenoliths were derived from a sedimentary unit underlying the Hyblean carbonate platform at about 8–10 km depth bsl. Instead, these rocks are strongly similar to the quartz arenite sequences of the Monte Soro flyschoid series that overly the Hyblean carbonates at ≤3–4 km depth beneath the volcano [*Michaud*, 1991]. Moreover, most of them preserved a fresh, unmetamorphosed aspect that demonstrates their short-lived interaction with the uprising magma. Therefore we rather suggest that these crustal xenoliths were mechanically extracted from shallower sedimentary horizons crossed by the erupted magma.

6. Conclusions

[53] The 2002–2003 flank eruption of Mount Etna constitutes the most explosive and longest eruptive phase culminating a 6 year period of intense summit activity initiated in mid-1995. The basalt produced by this eruption was the most primitive (MgO > 7wt %) on Etna since ∼240 years and probably represents the parental end-member responsible for the alkali enrichment observed in Etna lavas since 1974. This magma was very rich in volatiles, with an average dissolved H_2O content of 3.4 ± 0.2 wt %. It rose under closed system conditions from at least ∼10 km bsl until the surface, where it sustained powerful lava fountains during the initial stage of the eruption. Its sudden extrusion likely resulted from overpressuring of the shallow plumbing system several weeks before the eruption, but was facilitated by fractures already opened in 2001 and by ongoing eastward flank sliding of the volcano.

[54] Most of the lavas subsequently extruded were however derived from larger volumes of slightly more evolved,

trachybasaltic magma (MgO ~6 wt %) formed by crystal fractionation of the primitive basalt during temporary ponding at 6–4 km bsl. Such a source depth of the erupted magma is coherent with preeruptive seismic data. This magma was flushed by a deeper-derived CO_2-rich gas phase that promoted its partial dehydration during preeruptive ponding. The same process is suggested by inclusions that were trapped at greater depth of ~9 km bsl, where another magma ponding zone may occur. We thus conclude that magma dehydration driven by CO_2-rich bubble fluxing may be a common process on Mount Etna. This is an important and relatively new observation that may apply to other alkali basaltic volcanoes fed by CO_2-rich magmas.

[55] Finally, the volatile budget of the eruption, computed from the volumes of erupted magma and the amount of dissolved volatiles, shows no or limited excess sulphur degassing. This implies no preeruptive SO_2 accumulation and a prevalently closed system bulk degassing process. We show indeed that sulphur exsolution from Etna basalt becomes significant at only low pressure $\leq$150 MPa, when magma reaches the shallow plumbing system ($\leq$3 km bsl). This information places important constraints on the interpretation of the variations of both SO_2 flux and S/Cl ratio monitored in Etna gas emissions.

[56] **Acknowledgments.** We thank O. Belhadj for her help in preparing the samples, C. Sanchez-Garrido for her contribution to some analytical work and the nuclear microprobe team (Laboratoire Pierre Sue) for their assistance during experiments. Fruitful discussions with our colleagues in INGV-Catania are acknowledged. Rock sampling benefited from occasional helicopter assistance of the Italian Civil Defense. Two anonymous reviewers provided perceptive and insightful reviews that greatly contributed to the quality of this work.

References

Acocella, V., and M. Neri (2003), What makes flanks eruptions? The 2001 Etna eruption and its possible triggering mechanisms, *Bull. Volcanol.*, *65*, 517–529, doi:10.1007/s00445-003-0280-3.

Acocella, V., B. Behncke, M. Neri, and S. D'Amico (2003), Link between major flank slip and 2002–2003 eruption at Mt. Etna (Italy), *Geophys. Res. Lett.*, *30*(24), 2286, doi:10.1029/2003GL018642.

Aiuppa, A., C. Federico, A. Paonita, G. Pecoraino, and M. Valenza (2002), S, Cl and F degassing as an indicator of volcanic dynamics: The 2001 eruption of Mount Etna, *Geophys. Res. Lett.*, *29*(11), 1559, doi:10.1029/2002GL015032.

Allard, P. (1997), Endogenous magma degassing and storage at Mount Etna, *Geophys. Res. Lett.*, *24*, 2219–2222.

Allard, P. (1999), Mitigation of volcanic risks by remote sensing, *Final Rep. ENV4-CT96-288*, 55 pp., Eur. Commun. Res., Brussels, Belgium.

Allard, P., J. Carbonnelle, D. Dajlevic, J. C. Le Bronec, P. Morel, J. M. Maurenas, M. C. Robe, R. Faivre-Pierret, J. C. Sabroux, and P. Zettwoog (1991), Eruptive and diffuse emissions of carbon dioxide from Etna volcano, *Nature*, *351*, 387–391.

Allard, P., P. Jean-Baptiste, W. D'Alessandro, F. Parello, B. Parisi, and C. Flehoc (1997), Mantle-derived helium and carbon in groundwaters and gases of Mount Etna, Italy, *Earth Planet. Sci. Lett.*, *148*, 501–516.

Allard, P., M. Burton, and F. Muré (2005), Spectroscopic evidence for a lava fountain driven by previously accumulated magmatic gas, *Nature*, *433*, 407–410, doi:10.1038/nature03246.

Aloisi, M., A. Bonaccorso, S. Gambino, M. Mattia, and G. Puglisi (2003), Etna 2002 eruption imaged from continuous tilt and GPS data, *Geophys. Res. Lett.*, *30*(23), 2214, doi:10.1029/2003GL018896.

Alparone, S., D. Andronico, S. Giammanco, and L. Lodato (2004), A multidisciplinary approach to detect active pathways for magma migration and eruption at Mt. Etna (Sicily, Italy) before the 2001 and 2002–2003 eruptions, *J. Volcanol. Geotherm. Res.*, *136*(1–2), 121–140, doi:10.1016/j.jvolgeores.2004.05.014.

Anderson, A. T. (1974), Chlorine, sulfur and water in magmas and oceans, *Am. Bull. Geol. Soc.*, *85*, 1485–1492, doi:10.1130/0016-7606(1974)85<1485:csawim>2.0.co;2.

Andres, R. J., and A. D. Kasgnoc (1998), A time-averaged inventory of subaerial volcanic sulfur emissions, *J. Geophys. Res.*, *103*(D19), 25,251–25,262.

Andronico, D., et al. (2005), A multi-disciplinary study of the 2002–03 Etna eruption: Insights into a complex plumbing system, *Bull. Volcanol.*, *67*, 314–330, doi:10.1007/s00445-004-0372-8.

Barberi, F., L. Civetta, P. Gasparini, F. Innocenti, R. Scandone, and L. Villari (1974), Evolution of a section of the Africa- Europe plate boundary: Paleomagnetic and volcanological evidence from Sicily, *Earth Planet. Sci. Lett.*, *22*, 123–132, doi:10.1016/0012-821x(74)90072-7.

Behncke, B., and M. Neri (2003), The July–August 2001 eruption of Mt Etna (Sicily), *Bull. Volcanol.*, *65*, 461–476, doi:10.1007/s00445-003-0274-1.

Bianchi, F., S. Carbone, M. Grasso, G. Invernizzi, F. Lentini, G. Longaretti, S. Merlini, and F. Mostardini (1987), Sicilia orientale: Profilo geologico Nebrodi-Iblei, *Mem. Soc. Geol. Ital.*, *38*, 429–458.

Bonaccorso, A. (2001), Mt Etna volcano: Modelling of ground deformation patterns of recent eruptions and considerations on the associated precursors, *J. Volcanol. Geotherm. Res.*, *109*, 99–108, doi:10.1016/s0377-0273(00)00306-1.

Bonaccorso, A., and P. M. Davis (2004), Modeling of ground deformation associated with recent lateral eruptions: Mechanics of magma ascent and intermediate storage at Mt. Etna, in *Mt. Etna: Volcano Laboratory*, *Geophys. Monogr. Ser.*, vol. 143, edited by A. Bonaccorso et al., pp. 293–320, AGU, Washington, D. C.

Botcharnikov, R., M. Freise, F. Holtz, and H. Berhens (2005), Solubility of C-O-H mixtures in natural melts: New experimental data and application range of recent models, *Ann. Geophys.*, *48*(4–5), 633–646.

Burton, M., P. Allard, F. Murè, and C. Oppenheimer (2003a), FTIR remote sensing of fractional magma degassing at Mt. Etna, Sicily, in *Volcanic Degassing*, edited by C. Oppenheimer, D. M. Pyle, and J. Barclay, *Geol. Soc. Spec. Publ.*, *213*, 281–293.

Burton, M., F. Mure, G. Sawyer, and P. Allard (2003b), FTIR measurements of the 2002/2003 flank eruption of Mt. Etna, paper presented at AGU-EGS-EGU Assembly, Nice, 6–11 April.

Caltabiano, T., R. Romano, and G. Budetta (1994), SO_2 flux measurements at Mount Etna, Sicily, *J. Geophys. Res.*, *99*(D6), 12,809–12,819.

Caltabiano, T., G. G. Salerno, N. Bruno, and V. Longo (2003), Mt. Etna SO_2 emissions during the 2002–2003 eruption, paper presented at AGU-EGS-EGU Assembly, Nice, 6–11 April.

Caltabiano, T., M. Burton, S. Giammanco, P. Allard, N. Bruno, F. Murè, and R. Romano (2004), Volcanic gas emission from the summit craters and flanks of Mt. Etna, 1987–2000, in *Mt. Etna: Volcano Laboratory*, *Geophys. Monogr. Ser.*, vol. 143, edited by B. Calvari et al., pp. 111–128, AGU, Washington, D. C.

Calvari, S., M. Neri, and H. Pinkerton (2003), Effusion rate estimations during the 1999 summit eruption on Mount Etna, and growth of two distinct lava flow fields, *J. Volcanol. Geotherm. Res.*, *119*(1–4), 107–123, doi:10.1016/s0377-0273(02)00308-6.

Chiarabba, C., A. Amato, E. Boschi, and F. Barberi (2000), Recent seismicity and tomographic modelling of the Mt Etna plumbing system, *J. Geophys. Res.*, *105*(B5), 10,923–10,938.

Clocchiatti, R., J. L. Joron, and M. Treuil (1988), The role of selective alkali contamination in the evolution of recent historic lavas of Mt. Etna, *J. Volcanol. Geotherm. Res.*, *34*, 241–249, doi:10.1016/0377-0273(88)90036-4.

Clocchiatti, R., J. Weisz, M. Mosbah, and J. C. Tanguy (1992), Coexistence de verre alcalins et tholeitiques saturés en CO_2 dans les olivines d'Ici Castello (Etna, Sicile, Italie). Arguments en faveur d'un manteau anormal et d'un réservoir profond, *Acta Vulcanol.*, *2*, 161–173.

Clocchiatti, R., M. Condomines, N. Guénot, and J.-C. Tanguy (2004), Magma changes at Mount Etna: The 2001 and 2002–2003 eruptions, *Earth Planet. Sci. Lett.*, *226*, 397–414, doi:10.1016/j.epsl.2004.07.039.

Condomines, M., J. C. Tanguy, and V. Michaud (1995), Magma dynamics at Mt Etna: Constraints from U-Th-Ra-Pb radioactive disequilibria and Sr isotopes in historical lavas, *Earth Planet. Sci. Lett.*, *132*, 25–41, doi:10.1016/0012-821x(95)00052-e.

Corsaro, R. A., and M. Pompilio (2004a), Dynamics of magmas at Mount Etna, in *Mt. Etna: Volcano Laboratory*, *Geophys. Monogr. Ser.*, vol. 143, edited by B. Calvari et al., pp. 91–110, AGU, Washington, D. C.

Corsaro, R. A., and M. Pompilio (2004b), Buoyancy-controlled eruption of magmas at Mt Etna, *Terra Nova*, *16*(1), 16–22, doi:10.1046/j.1365-3121.2003.00520.x.

Dixon, J. E. (1997), Degassing of alkalic basalts, *Am. Mineral.*, *82*, 368–378.

Gambino, S., A. Mostaccio, D. Patanè, L. Scarfì, and A. Ursino (2004), High precision locations of the microseismicity preceding the 2002–2003 Mt. Etna eruption, *Geophys. Res. Lett.*, *31*(18), L18604, doi:10.1029/2004GL020499.

Ghiorso, M. S., and R. O. Sack (1995), Chemical transfer in Magmatic Processes IV, *Contrib. Mineral. Petrol.*, *119*(2–3), 197–212, doi:10.1007/s004100050036.

Giordano, D., and D. B. Dingwell (2003), Viscosity of hydrous Etna basalt: Implications for Plinian-style basaltic eruptions, *Bull. Volcanol.*, *65*, 8–14, doi:10.1007/s00445-002-0233-2.

Gvirtzamn, Z., and A. Nur (1999), The formation of Mount Etna as a consequence of the slab rollback, *Nature*, *401*, 782–785, doi:10.1038/44555.

Laigle, M., A. Hirn, M. Sapin, J. C. Lépine, J. Diaz, J. Gallart, and R. Nicolich (2000), Mount Etna dense array local earthquake P and S tomography and implications for volcanic plumbing, *J. Geophys. Res.*, *105*(B9), 21,633–21,646.

Lentini, F. (1982), The geology of the Mt. Etna basement, *Mem. Soc. Geol. Ital.*, *23*, 7–25.

Métrich, N., and R. Clocchiatti (1989), Melt inclusion investigation of the volatile behavior in historic alkaline magmas of Etna, *Bull. Volcanol.*, *51*, 185–198.

Métrich, N., and R. Clocchiatti (1996), Sulfur abundance and its speciation in oxidized alkaline melts, *Geochim. Cosmochim. Acta*, *60*, 4151–4160, doi:10.1016/s0016-7037(96)00229-3.

Métrich, N., and M. J. Rutherford (1998), Low pressure crystallization paths of H_2O-saturated basaltic-hawaiitic melts from Mt Etna: Implications for open-system degassing volcanoes, *Geochim. Cosmochim. Acta*, *62*, 1195–1205, doi:10.1016/S0016-7037(98)00048-9.

Métrich, N., R. Clocchiatti, M. Mosbah, and M. Chaussidon (1993), The 1989–90 activity of Etna. Magma mingling and ascent of a H_2O-Cl-S rich basalt. Evidence from the melt inclusions, *J. Volcanol. Geotherm. Res.*, *59*, 131–144, doi:10.1016/0377-0273(93)90082-3.

Métrich, N., A. Bertagnini, P. Landi, and M. Rosi (2001), Crystallization driven by decompression and water loss at Stromboli volcano (Aeolian Islands, Italy), *J. Petrol.*, *42*, 1471–1490, doi:10.1093/petrology/42.8.1471.

Métrich, N., P. Allard, N. Spilliaert, D. Andronico, and M. Burton (2004), 2001 flank eruption of the alkali- and volatile-rich primitive basalt responsible for Mount Etna's evolution in the last three decades, *Earth Planet. Sci. Lett.*, *228*, 1–17, doi:10.1016/j.epsl.2004.09.036.

Michaud, V. (1991), L'enrichissement sélectif en K, Rb et Cs des laves récentes de l'Etna: Rôle des fluides du système phréatique dans l'interaction magma-encaissant sédimentaire et implications sur les dynamismes éruptifs, Ph.D. thesis, 554 pp., Univ. Orsay, France.

Monaco, C., S. Catalano, O. Cocina, G. De Guidi, C. Ferlito, S. Gresta, C. Musumeci, and L. Tortorici (2005), Tectonic control on the eruptive dynamics at Mt. Etna Volcano (Sicily) during the 2001 and 2002–2003 eruptions, *J. Volcanol. Geotherm. Res.*, *144*, 211–233, doi:10.1016/j.jvolgeores.2004.11.024.

Murru, M., C. Montuori, M. Wyss, and E. Privitera (1999), The locations of magma chambers at Mt Etna, Italy, mapped by b-values, *Geophys. Res. Lett.*, *26*, 2553–2556.

Neri, M., V. Acocella, and B. Behncke (2004), The role of the Pernicana Fault System in the spreading of Mt. Etna (Italy) during the 2002–2003 eruption, *Bull. Volcanol.*, *66*(5), 417–430, doi:10.1007/s00445-003-0322-x.

Neri, M., V. Acocella, B. Behncke, V. Maiolino, A. Ursino, and R. Velardita (2005), Contrasting triggering mechanisms of the 2001 and 2002–2003 eruptions of Mount Etna (Italy), *J. Volcanol. Geotherm. Res.*, *144*, 235–255, doi:10.1016/j.jvolgeores.2004.11.025.

Newman, S., and J. B. Lowenstern (2002), $V_{OLATILE}C_{ALC}$: A silicate melt-H_2O-CO_2 solution model written in Visual Basic Excel, *Comput. Geosci.*, *28*(5), 597–604, doi:10.1016/s0098-3004(01)00081-4.

Patanè, D., P. De Gori, C. Chiarabba, and A. Bonaccorso (2003), Magma ascent and the pressurization of Mount Etna's volcanic system, *Science*, *299*, 2061–2063, doi:10.1126/Science.1080653.

Pennisi, M., and M. Le Cloarec (1998), Variations of Cl, F, and S in Mount Etna's plume, Italy, between 1992 and 1995, *J. Geophys. Res.*, *103*(B3), 5061–5066.

Pompilio, M., and M. Rutherford (2002), Pre-eruption conditions and magma dynamics of recent amphibole-bearing Etna basalt, *Eos Trans. AGU*, *83*(47), Fall Meet. Suppl., Abstract V61A-1354.

Roedder, E. (1984), *Fluid Inclusions*, 646 pp., Mineral. Soc. of Am., Washington, D. C.

Schiano, P., R. Clocchiatti, L. Ottolini, and T. Busà (2001), Transition of Mount Etna lavas from a mantle-plume to an island-arc magmatic source, *Nature*, *412*, 900–904, doi:10.1038/35091056.

Sobolev, A. (1996), Melt inclusions in minerals as a source of principle petrological information, *Petrology*, *4*, 228–239.

Sobolev, A., and M. Chaussidon (1996), H_2O concentrations in primary melts from supra-subduction zones and mid-oceanic ridges: Implications for H_2O storage and recycling in the mantle, *Earth Planet. Sci. Lett.*, *137*, 45–55, doi:10.1016/0012-821x(95)00203-o.

Spilliaert, N. (2006), Dynamiques de remontée, dégazage et éruption des magmas basaltiques riches en volatils: Traçage par les inclusions vitreuses et modélisation des processus dans le cas de l'Etna, 2000–2002, Ph.D. thesis, 238 pp., Inst. du Phys. Globe Paris, 6 Jan.

Tanguy, J. C., M. Condomines, and G. Kieffer (1997), Evolution of the Mount Etna magma: Constraints on the present feeding system and eruptive mechanism, *J. Volcanol. Geotherm. Res.*, *75*, 221–250, doi:10.1016/s0377-0273(96)00065-0.

Tonarini, S., P. Armienti, M. D'Orazio, and F. Innocenti (2001), Subduction-like fluids in the genesis of Mt. Etna magmas: Evidence from boron isotopes and fluid mobile elements, *Earth Planet. Sci. Lett.*, *192*, 471–483, doi:10.1016/s0012-821x(01)00487-3.

Trouslard, P. (1995), PYROLE: Un logiciel au service des analyses par faisceau d'ions, *Rapp. CEA-R-5703*, 29 pp., Comm. à l'Energie At., Paris.

P. Allard, N. Métrich, and N. Spilliaert, Laboratoire Pierre Süe, UMR 9956 CNRS–CEA, CE Saclay, F-91191 Gif sur Yvette cedex, France. (nicole.metrich@cea.fr)

A. V. Sobolev, Max-Planck-Institut für Chemie, Postfach 3060, D-55020 Mainz, Germany.